One Earth

Article

Black-carbon-induced regime transition of boundary layer development strongly amplifies severe haze

Graphical abstract

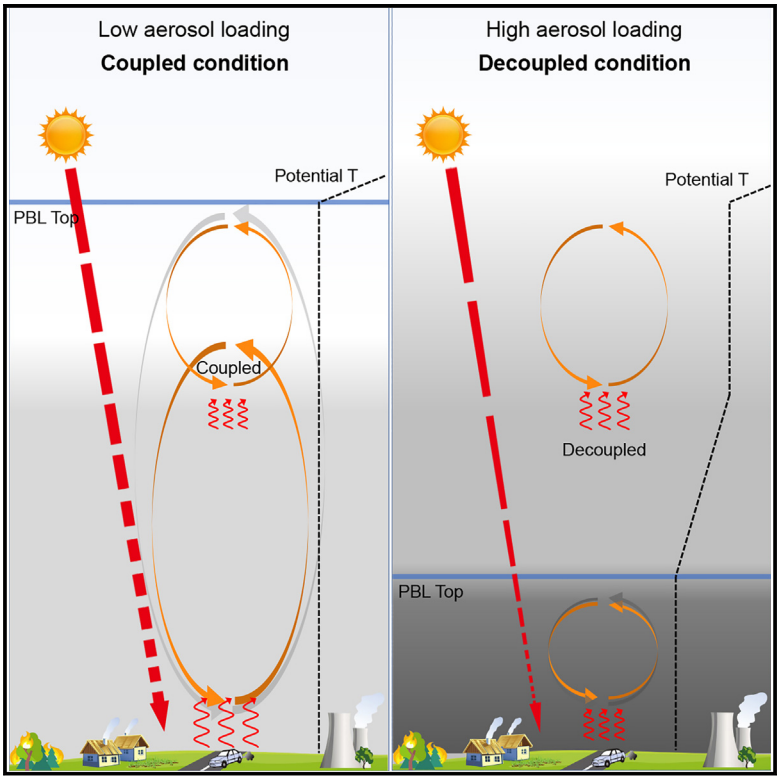

Highlights

- High concentration of black carbon (BC) can trigger a tipping point of PBL development
- With aerosol load above the tipping point, the maximum PBL height decreases abruptly
- The tipping point is caused by BC-induced decoupling of vertical mixing zones
- Reducing BC is much more efficient to avoid the tipping point than reducing other aerosols

Authors

Jiandong Wang, Hang Su, Chao Wei, ..., Meinrat O. Andreae, Ulrich Pöschl, Yafang Cheng

Correspondence

h.su@mpic.de (H.S.), yafang.cheng@mpic.de (Y.C.)

In brief

High concentration of absorbing aerosols such as black carbon (BC) can trigger a "tipping point" of planetary boundary layer (PBL) development through decoupling of vertical mixing zones. With aerosol concentration above the tipping point, the daily maximum PBL height decreases abruptly, and the shallow PBL traps more aerosols near the ground and greatly deteriorates air quality. To avoid reaching the tipping point, a targeted reduction of BC can be much more effective than reducing the total aerosol burden.

Wang et al., 2023, One Earth 6, 751–759
June 16, 2023
https://doi.org/10.1016/j.oneear.2023.05.010

CellPress

One Earth

CellPress
OPEN ACCESS

Article

Black-carbon-induced regime transition of boundary layer development strongly amplifies severe haze

Jiandong Wang,[1] Hang Su,[2,*] Chao Wei,[2] Guangjie Zheng,[1] Jiaping Wang,[3] Tianning Su,[4] Chengcai Li,[5] Cheng Liu,[6] Jonathan E. Pleim,[7] Zhanqing Li,[4] Aijun Ding,[3] Meinrat O. Andreae,[8,9,10] Ulrich Pöschl,[2] and Yafang Cheng[1,11,*]

[1]Minerva Research Group, Max Planck Institute for Chemistry, 55128 Mainz, Germany
[2]Multiphase Chemistry Department, Max Planck Institute for Chemistry, 55128 Mainz, Germany
[3]Joint International Research Laboratory of Atmospheric and Earth System Sciences, School of Atmospheric Science, Nanjing University, Nanjing 210023, China
[4]Department of Atmospheric and Oceanic Sciences, University of Maryland, College Park, MD 21029, USA
[5]Department of Atmospheric and Oceanic Sciences, Peking University, Beijing 100871, China
[6]Department of Precision Machinery and Precision Instrumentation, University of Science and Technology of China, Hefei 230026, China
[7]The U.S. Environmental Protection Agency, Research Triangle Park, NC 27711, USA
[8]Max Planck Institute for Chemistry, 55128 Mainz, Germany
[9]Scripps Institution of Oceanography, University of California San Diego, La Jolla, CA 92093, USA
[10]Department of Geology and Geophysics, King Saud University, Riyadh 11451, Saudi Arabia
[11]Lead contact
*Correspondence: h.su@mpic.de (H.S.), yafang.cheng@mpic.de (Y.C.)
https://doi.org/10.1016/j.oneear.2023.05.010

SCIENCE FOR SOCIETY Air pollution is a major threat to human health. Severe haze is often caused by an unexpected extremely shallow planetary boundary layer (PBL), the lowest part of the atmosphere where most pollutants are concentrated. Insufficient understanding of the formation mechanism of a shallow PBL leads to failure of air quality forecast and effective prevention. We found that high atmospheric concentrations of black-carbon (BC) particles (an aerosol) can trigger a "tipping point" in PBL height. Above this tipping point, high concentrations of these particles suppress vertical mixing of atmospheric layers and create a stable PBL, trapping pollutants near the ground and greatly deteriorating air quality. This scenario can be avoided through targeted reductions of BC emissions (rather than targeting total particulate matter reductions). Results further show that mega-wildfires through climate change and nuclear disasters can result in enormous BC emissions and cause extreme stratification of the atmosphere and persistent aerosol layers.

SUMMARY

Black-carbon (BC) aerosol can strongly influence planetary boundary layer (PBL) development and thus severe haze formation, but its distinct role compared with scattering aerosols is not yet fully understood. Here, combining numerical simulation and field observation, we found a "tipping point," where the daily maximum PBL height decreases abruptly when exceeding a critical threshold of aerosol optical depth (AOD), due to a BC-induced decoupling of mixing zones. Because the threshold AOD decreases with increasing BC mass fraction, our results suggest that the abrupt transition of PBL development to adverse conditions can be avoided by reducing the AOD below the threshold but can be avoided more efficiently by reducing the BC mass fraction to increase the threshold (e.g., up to four to six times more effective in extreme haze events in Beijing). To achieve co-benefits for air quality and climate change, our findings clearly demonstrate that high priority should be given to controlling BC emissions.

INTRODUCTION

In recent decades, heavy winter haze events have frequently occurred in Chinese megacity regions, threatening the health of millions.[1–4] Light-absorbing aerosols, such as black carbon (BC), can change the radiation budget, leading to a cooling of the Earth's surface and the near-surface atmosphere and a warming of the overlying polluted atmosphere.[5–8] BC also affects the climate by modulating snow albedo[9,10] and large-scale circulations.[11,12] Although BC has been widely recognized as an important agent

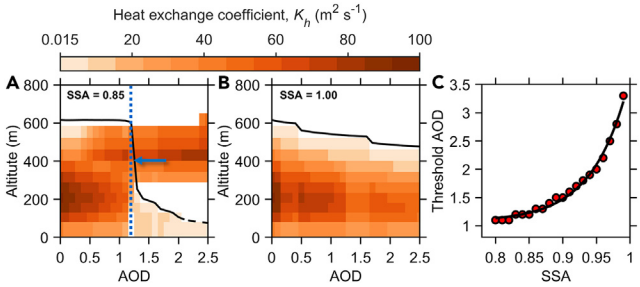

Figure 1. Impact of BC on aerosol-PBL interactions

(A) WRF-simulated maximum planetary boundary layer (PBL) height (black line) and vertical profile of corresponding heat exchange coefficient (K_h, color contour) as a function of aerosol optical depth (AOD). The aerosol single-scattering albedo (SSA) is set to 0.85. The blue dashed line and blue arrow mark the threshold AOD for a regime transition of aerosol-PBL interaction and abrupt change of the maximum PBL height in the presence of BC. The grid cells with K_h lower than 0.015 are set to white color.

(B) The same as in (A), but with SSA = 1.0.

(C) Threshold AOD values under different SSA scenarios.

in the global radiative budget and forcing,[13–16] its heating effect on the development of the atmospheric boundary layer is still not fully understood. The planetary boundary layer (PBL) is the lowest part of the troposphere that is directly influenced by the Earth's surface. The most common definition of PBL height is the height up to which the influence of the presence of the lower surface is detectable.[17] During daytime, the PBL is often a convective PBL, where the PBL height is largely driven by convections and is closely linked to the convective and turbulent diffusion of air pollutants. Several studies suggest that BC-induced heating will alter the turbulence strength, increase vertical thermal stability, suppress the PBL development, and thus aggravate air pollution.[5,18–25] On the other hand, BC-induced heating can also lift the top of the PBL, compensating the effects of reduced buoyancy underneath.[26–30] Moreover, light absorption and heating by BC aerosols within the PBL may also lead to an increase of vertical mixing rather than strengthened stratification.[31] BC also affects cloud distribution via aerosol-cloud interactions and aerosol-radiation interactions,[32,33] which may further influence the energy balance and dynamic in the PBL as well as meteorology and aerosols below the cloud. Here, we revisit this topic by comprehensive investigations of aerosol-PBL interactions through single-column model simulations using the Weather Research and Forecasting Model (WRF) and the online coupled WRF and chemistry model (WRF-Chem), where a wide range of scenarios with different meteorological conditions and aerosol properties (concentration, single-scattering albedo [SSA], and vertical distribution) have been studied (Figure S1). We find a BC-induced sharp regime transition of aerosol-PBL interactions that explains the formation of a shallow PBL and amplifies the severe winter haze events in polluted megacity regions in northern China.

RESULTS

BC-induced tipping point of PBL

Figure 1A shows the response of PBL structure to a change of aerosol optical depth (AOD) under stagnant weather conditions and with SSA = 0.85, characteristic for winter haze events in Beijing and the North China Plain (see Figure S1). We find a tipping point of the daily maximum PBL height (H_{max}) (black line in Figure 1A) response to increasing AOD when aerosol loads exceed a certain threshold (AOD ~ 1.2), suggesting a transition in the aerosol-PBL interaction regimes. According to long-term statistics,[34,35] AOD of ~1.2 in this area corresponds, on average, to a surface fine particulate matter ($PM_{2.5}$) concentration of ~100–200 μg m^{-3} in winter.[34] The threshold AOD (blue dashed line in Figure 1A) marks two distinct regimes of aerosol-PBL interaction. In the low-AOD regime (AOD ≤ 1.2), increasing AOD has almost no effect on H_{max}. When crossing the threshold, an AOD change of 0.1 unit leads to a drop of H_{max} from ~600 to ~200 m, showing an extremely strong effect on the PBL. Such a regime transition is also evident from a similar prompt change of heat exchange coefficients (K_h, colored contour in Figure 1A), which reflect the intensity of turbulent mixing, a key parameter controlling the dispersion of air pollutants. To the best of our knowledge, this is the first time such a regime transition and collapse of PBL has been revealed.

As shown in Figures 1A and 1B, this tipping point of the PBL development is a unique feature in the presence of light-absorbing BC aerosols. Increasing AOD of non-absorbing aerosols (i.e., SSA = 1.0, purely light scattering) only leads to a continuous moderate reduction of H_{max} and K_h (Figures 1B and S2). The importance of BC is also evident from its strong impact on the threshold AOD. As shown in Figure 1C, increasing SSA (i.e., decreasing BC mass fraction) from 0.8 to 0.95 will increase the threshold AOD by a factor of ~2, strongly reducing the probability of the aerosol-induced abrupt decrease of PBL height. Further sensitivity studies with both WRF and WRF-Chem models show that, in the presence of light-absorbing BC aerosols, the existence of a threshold is not limited to specific meteorological conditions, vertical aerosol distributions, or boundary layer model scheme but can be found over other weather conditions, locations, and seasons (Figures S3A–S3C, S3H, S3I, S4, and S5), suggesting a commonly existing mechanism. Although the threshold value can be different, a tipping point is always observed. According to these results, weaker solar radiation will lead to a lower threshold AOD and a higher tendency of the abrupt decrease of PBL height (Figures S3B, S3D, and S3E), which means that this mechanism may play an important role in the severe haze formation in wintertime in northern China.

Figure 2A shows the observed response of daytime PBL development on aerosol loading in winter Beijing, based on micropulse lidar (MPL) measurements in December, January, and February from December 2016 to February 2018 (see section "experimental procedures"). For comparison, we also performed WRF column model simulations for the same period (see section "experimental procedures" and supplemental information). In accordance with the model simulations (Figures 2B and 2C), the observations exhibit a similar threshold AOD (~0.5–0.75) and two distinct regimes of aerosol-PBL interaction. On average, for the winter period, the modeled PBL height in Beijing decreases by around 50% when AOD exceeds the threshold (Figure 2C), which is consistent with the observation (Figure 2A). These results further support the proposed mechanism (i.e., BC-induced regime transition of boundary layer development).

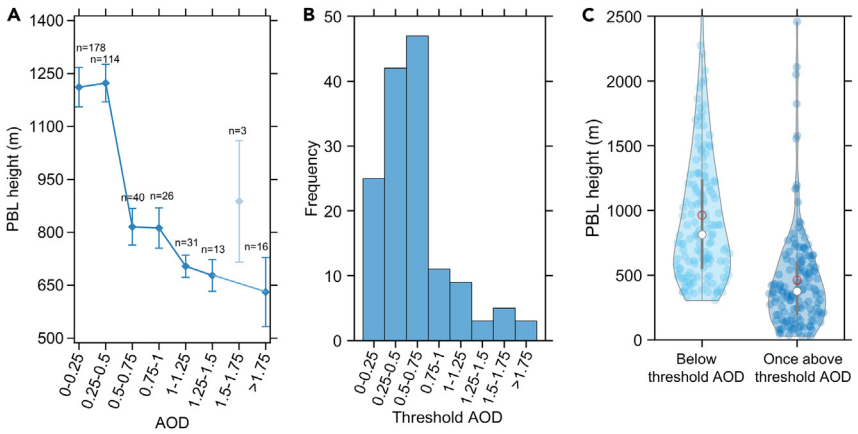

Figure 2. Observed and modeled response of PBL development on aerosol loading in winter Beijing

(A) Observed daytime PBL height versus corresponding AOD in winter Beijing (December, January, and February from December 2016 to February 2018, as detailed in the text). Diamonds represent the mean value, and the whiskers show the standard error of mean. The number of samples (n) in each bin is also marked. The blue line shows the overall pattern, and the point at AOD = 1.5–1.75 (light blue diamond) is omitted in the trend analyses because of low statistic (n = 3) and large error in that bin.

(B) Frequency of the simulated threshold AOD (tipping point). Model simulations are performed for the same periods as the observation.

(C) Distributions of simulated maximum PBL heights below and once above the threshold AOD. The white and red dots represent median values and mean values, respectively, and the thick gray bars mark the respective 25th and 75th percentile (top and bottom edges). Thin bars are the rest of the distribution except the outliers. The shaded areas represent the probability density of the data populations. The blue dots show the data collected for the violin plot.

The BC-induced abrupt change of the PBL height is in contrast to the conventional understanding of aerosol-PBL interactions, where a gradual increase of aerosol loading is expected to cause a continuous reduction of surface net solar radiation (R_n) and surface sensible heat flux (F_h), and thus a continuous reduction of the PBL height. As shown in Figure S8, R_n and F_h do show a gradual change against AOD in the presence of BC. Then, the question is why does the PBL respond differently crossing a certain threshold AOD?

Decoupling of mixing zones

To answer this question and understand the underlying mechanism, we investigated the diurnal evolution of the PBL and the mixing structure below, around, and above the threshold AOD (Figures 3 and S9). As indicated by K_h, the presence of absorbing aerosols leads to the development of two mixing zones: one near the ground driven by surface heating, and another one at higher altitude driven by heating of absorbing BC aerosols. At a given SSA, increasing aerosol loading has distinct effects on the two mixing zones. On one hand, it suppresses the development of the lower zone by reducing the surface heat flux through dimming effect[29] and reduction of temperature gradient between the surface and atmosphere. On the other hand, it promotes the development of the upper zone by providing additional buoyancy and inducing convection above the aerosol layers through increasing light absorption at higher altitude (Figure S10A). A similar invigoration effect of layered BC has been investigated for aviation and biomass-burning smoke plumes.[36–39]

At an AOD below the threshold (Figures 3A and 3B), the two mixing zones are coupled to each other in the course of boundary layer development, reaching a maximum PBL height (H_{max}) of ~600 m around noontime. In this regime (AOD $\leq$ 1.2), despite of the upper-level heating (actually a gradient in the aerosol heating; Figure S10A) and surface dimming (Figure S8A), the uniform potential temperature θ around 15:00 is a clear proof that the strong mixing effect is able to eliminate the daytime gradient and dilute air pollutants emitted at the surface by upward transport (black dashed line and two blue lines in Figure 2E). As long as the two zones are coupled, the increased mixing in the upper zone and inter-zonal transport compensates for the reduced mixing in the lower zone, leading to an insensitive response of H_{max} and mean K_h to the increase of AOD (Figures 1A, S2, S3F, and S3G). As shown in Figures 1A and 1B, compared with scattering aerosols (SSA = 1.0), the absorbing aerosol have a much weaker effect in terms of "suppressing" the boundary layer development in this regime, and, when the BC mass fraction further increases (e.g., SSA = 0.8), it may even slightly enhance the boundary layer development prior to the tipping point (Figures S2 and S4).

At an AOD above the threshold (Figures 3C and 3D), the development of the lower mixing zone is suppressed so strongly that it cannot connect to the upper one. Such decoupling leads to a sharp drop of H_{max} (Figure 1A) and a regime transition of aerosol-PBL interactions. Under this condition, θ shows a large inter-zonal difference, which forms a noontime inversion above the surface zone and suppresses further development of the PBL in the afternoon (orange and red line in Figures 3E and S11). After decoupling, BC aerosols lead to much lower PBL height than scattering aerosol for the same AOD. As shown in Figures 1A and 1B, for an AOD of 1.5, scattering aerosols lead to a PBL height of ~530 m, while the presence of BC aerosols results in a much shallower PBL of ~190 m. The stronger suppression effect by BC-containing aerosols can be explained by two reasons: (1) first, the light absorption effect is more efficient than the light scattering effect in reducing surface incoming solar radiation, the energy source of surface heating. The absorbed solar radiation is fully lost and cannot reach the surface anymore, while only part of the scattered solar radiation is reflected back to the space and the rest will reach the surface. As shown in Figure S8A, given the same AOD or aerosol extinction (the sum of scattering and absorption), BC aerosols lead to much less incoming surface solar radiation than scattering aerosols. (2) BC-induced heating of atmosphere further reduces the surface heat flux. The heat flux from surface heats the bottom air, resulting in convections and driving the development of PBL. When BC heats the air, it reduces the temperature difference between

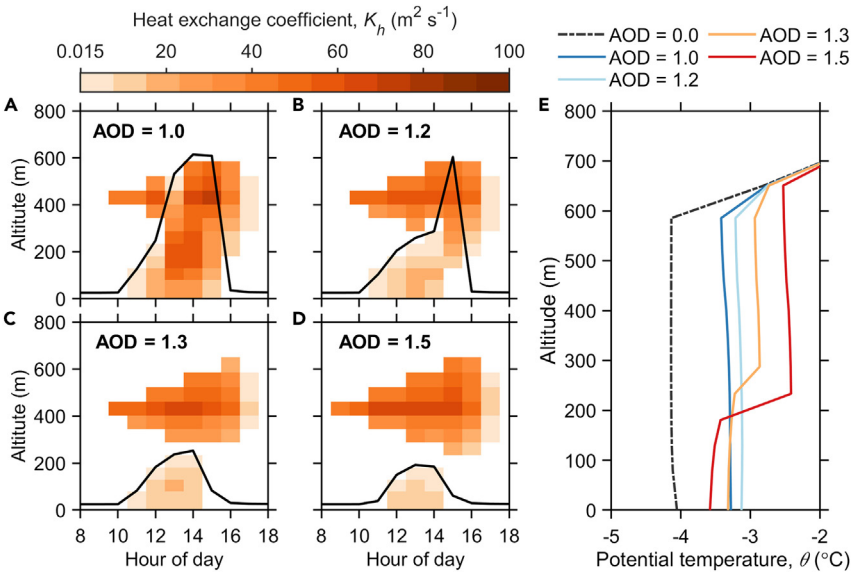

Figure 3. Coupling and decoupling of the mixing zones determine the diurnal evolution of PBL

(A) Diurnal variation of PBL height (black line) and vertical profile of heat exchange coefficient (K_h, color contour) with SSA = 0.85 and AOD = 1.0. Grid cells with K_h lower than 0.015 are set to white color.

(B) The same as in (A), but with AOD = 1.2.

(C) The same as in (A), but with AOD = 1.3.

(D) The same as in (A), but with AOD = 1.5.

(E) Corresponding vertical profiles of potential temperature (θ) at 15:00 (local time).

surface and the atmosphere. So, even for the same incoming solar radiation, the heat flux in the presence of BC is still smaller than that for scattering aerosols (Figure S8B), which further suppresses the development of the lower mixing zone.

In this decoupled regime (AOD > 1.2), air pollutants are trapped within the lower mixing zone, and BC aerosols start to suppress the development of the PBL much more efficiently than scattering aerosols. As shown in Figures 1A and 1B, a ~100-m decrease of H_{max} requires only a 0.5-unit change of AOD in the presence of elevated BC mass fractions (SSA = 0.85), compared with a ~1.7-unit change for purely scattering aerosols (SSA = 1.0). The stronger effect of BC aerosols in this regime can be attributed to three factors: a smaller forward scattering to extinction ratio, resulting in less solar radiation reaching the ground under the same AOD (Figure S5); additional heating of the atmosphere, reducing the air-surface temperature gradient and heat fluxes (Figure S9B); and a strengthened inversion induced by BC in the residual layer in the morning, retarding the full development of the PBL (Figure S11).

Our finding reconciles the contrasting results in early studies, where the coupled regime (Figure 3A) corresponds to a weak suppression or even slight invigoration effect of BC on the PBL,[5,22–25] whereas a strong suppression effect[6,14–16,40,41] can be expected in the decoupled regime (Figure 4B). Our results show that aerosol-induced upper-air heating and surface dimming does not necessarily lead to an inversion or strengthened stratification, as in the coupled regime. However, once the two mixing zones are decoupled, the PBL development will be strongly suppressed, and an inversion will form. Under stagnant weather conditions, the strong suppression of PBL development may lead to such an unfavorable dispersion condition during daytime, which resembles the stable boundary layer condition at nighttime (Figure 1A). This mechanism may help to explain the observed nonlinear dependence of PBL height on AOD in Beijing (i.e., an abrupt change of PBL height at certain AOD levels; Figure 2A). By reanalyzing the data of Ding et al.,[19] we find that the regional modeling results also support our finding of a BC-induced regime transition of aerosol-PBL interactions (Figure S15): in the presence of BC aerosols, the PBL height is almost insensitive to the reduction of surface heat flux (ΔR_n) until $\Delta R_n \sim 20$ W m^{-2}, but becomes much more sensitive than that of pure scattering aerosols when $\Delta R_n > \sim 20$ W m^{-2}; in contrast, with pure scattering aerosols, the PBL height shows a moderate nearly linear dependence over the whole ΔR_n range.

Implications for air-pollution controls

The BC-induced tipping point and regime transition of PBL development have important implications for the development of air-pollution control strategies. To the best of our knowledge, this is the first time such a regime transition and a tipping point of PBL development has been revealed. By keeping AOD below the threshold, one can prevent the BC-induced abrupt decrease of PBL height and avoid a further increase of $PM_{2.5}$ concentrations due to a lack of convective dilution (Figures 1A and S16). The large marginal effect across the threshold makes it a prime target for emission control, especially under winter haze conditions in the North China Plain. To stay below the threshold of abrupt decrease of PBL height, two alternative pathways can be taken, as illustrated Figure 5: (1) reduce the total aerosol burden and AOD, or (2) increase the aerosol SSA and the AOD threshold AOD. The latter can be achieved by selectively reducing the emission of light-absorbing aerosols such as BC-containing particles. Examples of how an abrupt decrease of PBL height could be avoided under severe winter haze conditions in Beijing are given in Figure 5B. Path 1 would require a ~40% reduction of total aerosol burden and AOD, while path 2 would require a ~60%–70% reduction of BC corresponding to a ~7%–10% reduction of AOD, depending on BC mixing state (see section "experimental procedures"). This means a targeted reduction of BC can be four to six times more effective than reducing the total aerosol burden. The much smaller reduction of total aerosol burden and AOD required for path 2 is due to an ~10% increase of SSA (from 0.85 to 0.94), which leads to a ~50% increase of threshold AOD for the boundary layer collapse (from 1.2 to 1.8). In practice, a targeted reduction of BC and corresponding increase of SSA could be achieved by reducing emission from diesel exhaust and low-efficiency domestic heating etc., which are major sources of BC in the North China Plan. Since BC is an important short-lived global warming agent, a targeted

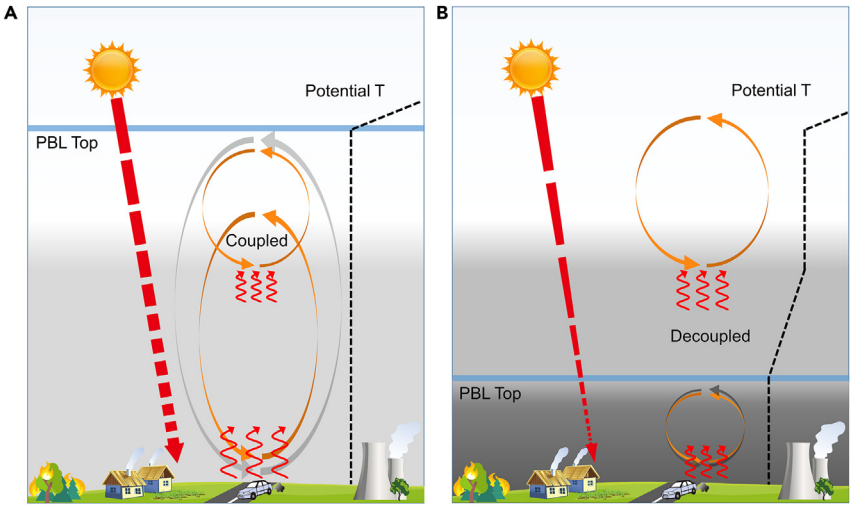

Figure 4. BC-induced abrupt change of PBL height and prompt regime transition of aerosol-PBL interactions

(A) Scenario with low AOD or high aerosol SSA when the two mixing zones (orange circles of arrows) are coupled and the PBL is well developed.

(B) Scenario with high AOD or low SSA, when the two mixing zones (orange circles of arrow) are decoupled and the PBL development is suppressed. The thick blue lines mark the PBL top. The red dashed lines show the changes of solar radiation. The red waved arrows indicate either surface heating or heating in the atmosphere by BC. The gray circles of arrows represent the mixing processes within the PBL. The black dashed lines on the right side of each panel show the vertical profiles of potential temperature.

reduction of BC emissions may also help to compensate for the temperature rise expected from improving air quality by removing aerosols,[42] leading to co-benefits for public health and the mitigation of climate change in the Anthropocene.[43–49]

EXPERIMENTAL PROCEDURES

Resource availability

Lead contact

Further information and requests for resources and reagents should be directed to and will be fulfilled by the lead contact, Yafang Cheng (yafang.cheng@mpic.de).

Materials availability

This study did not generate new unique materials.

Data and code availability

All data needed to evaluate the conclusions in the paper are present in the paper and/or the supplemental materials. The data that produced all figures in this study are available from Figshare database: https://doi.org/10.6084/m9.figshare.22678720. All data for the figures in the supplemental information are available from the lead contact upon reasonable request. Custom code for this work is available from the lead contact upon reasonable request.

Model setup

In this study, we used the single column model (SCM) version of the WRF (https://www.mmm.ucar.edu/weather-research-and-forecasting-model) v3.8.1 and WRF-Chem[50] to simulate and investigate the aerosol planetary boundary layer (PBL) interactions. The SCM simulates all physical and chemical processes in the same way as in a standard simulation of WRF/WRF-Chem. In both WRF and WRF-Chem simulations, the radiation, microphysics, and land surface modules were configured as Rapid Radiative Transfer Model for Global Circulation Models (RRTMG) for long wave and short wave,[51] Morrison 2-moment,[52] and Noah[53] schemes, respectively. The Asymmetric Convective Model version 2 (ACM2) boundary layer scheme, which considers both local and non-local closure, was adopted in this study.[54] In the ACM2 scheme, the PBL height is diagnosed as the height above the level of neutral buoyancy where bulk Richardson number computed for the entrainment layer exceeds the critical value (0.25 over the land[54]). We extracted the values of the heat exchange coefficients (K_h) before partitioning into local and non-local components in the convective boundary layer. Therefore, the values of K_h are representative of all turbulent mixing. Note that, above the boundary layer, there is no non-local component; thus, all turbulent mixing is by eddy diffusion. In WRF-Chem, the gas-phase reactions were simulated with the Model of Ozone and Related Chemical Tracers (MOZART) module.[55] The four-bin sectional Model for Simulating Aerosol Interactions and Chemistry (MOSAIC) aerosol module[56] was adopted and the aerosol optical properties were simulated with core-shell Mie theory.[57]

The simulation domain was set as 3 × 3 horizontal grids with a 4-km grid size. We adopted 60 vertical eta layers from the surface to 200 hPa (~12 km) with 16 layers below 1 km. Each simulation started from 20:00 (Beijing local time, coordinated universal time [UTC + 8]) 1 day before the target day. The initial condition of the soil was extracted from a nested three-dimensional (3D) WRF model simulation derived from the NCEP FNL Operational Global Analysis data.[58] The vertical profile of atmospheric conditions was initialized by the sounding data (http://weather.uwyo.edu/upperair/sounding.html). Periodic boundary conditions in the horizontal direction were used.

In WRF column model simulations, the effects of light absorption of BC aerosols were reflected/accounted for by the aerosol optical thickness and SSA, as well as asymmetry factor in each model layer. In the base case, we increased AOD from 0.0 to 6.0 with an increment of 0.1 and varied the SSA from 1.0 (pure scattering, no BC) to 0.6 (strongly absorbing), which covers most of the cases according to a series of observations (Figure S1C). The SSA was set as 0.85 in Figure 1A, representing the average fraction of absorbing aerosols in Beijing and the North China Plain, which varies from 0.80 to 0.90 (Figure S1C). The asymmetry factor was set to be 0.65 in the WRF scenarios.

In the WRF simulations, the influence of aerosols on PBL development was achieved by different scenarios of prescribed aerosol layers. However, in WRF-Chem, the vertical distributions of aerosols were calculated rather than prescribed as in the case of WRF simulations, which allows us to see the relative changes in both PBL structure and surface $PM_{2.5}$ concentration.

Long-term statistical analyses were performed to obtain the response of PBL development on aerosol loading in winter Beijing based on observational data. As detailed in Su et al.,[59] the daytime PBL height is derived from ground-based micropulse lidar (MPL) measurements in Beijing (39.99°N, 116.31°E), and AOD data are version 3, level 1.5 product from the AERONET site (40°N, 116.38°E). The winter season data include observations in December, January, and February from December 2016 to February 2018. For a better statistic, we used daytime lidar observations from 12:00 to 16:00 (local time) to derive the daytime PBL height,[59] and Figure 2A shows a similar pattern compared with the results when only data from 13:00 to 15:00 were used (Figure S12).

Base cases

The base case was conducted for Beijing (39.9°N, 116.4°E) on January 11, 2013, a typical stagnant weather condition in wintertime in Beijing.[2,60] Without perturbation from aerosols, i.e., AOD = 0, the model-simulated maximum PBL height (H_{max}) on this day was ~600 m, which is an average level of daily H_{max} in Beijing reported by Zhang and Cao.[61]

To investigate the impact of aerosols on the PBL development, aerosols were considered to be uniformly distributed below 460 m based on lidar observation at 20:00 on the day before January 11, 2013[62] (Figures S1A and S1B).

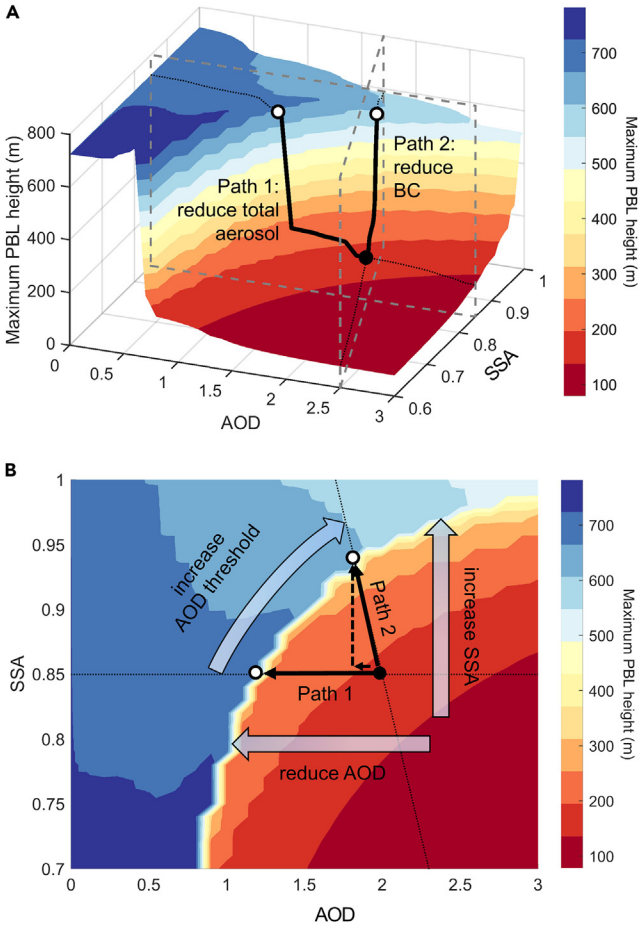

Figure 5. Mapping of mitigation measures in Beijing, to reduce AOD or reduce BC to increase SSA and threshold AOD

(A) The 3D representation of the response of maximum PBL height to the changes of AOD and SSA. The black dot is an exemplary case in winter Beijing (base case) with strongly suppressed PBL in the decoupled regime. The open circles indicate the restored PBL after implementing mitigation measures. Path 1 represents the reduction of total AOD at a constant SSA. Path 2 represents the reduction of BC aerosols only. The cross section of path 2 is not perpendicular to the x axis of AOD, because reducing BC will lead to changes in both AOD and SSA. The corresponding change of SSA and AOD to the reduction of BC is mapped according to an offline optical Mie model calculation with the assumption of externally mixed BC particles (see section "experimental procedures").

(B) The same as in (A), but with 2D representation. Compared with path 1, path 2 requires less change of AOD because of the corresponding enhancement of SSA and increase of the threshold AOD when reducing BC particles.

The aerosol SSA was set as 0.85, representing the average fraction of absorbing aerosols in Beijing and the North China Plain, which varies from 0.80 to 0.90[63] (Figure S1C). While the asymmetry factor was set to be 0.65 in the WRF scenarios,[64] its value depends on aerosol species and concentration.

To study the effect of aerosol loading and absorbing BC particles on aerosol-PBL interactions, we performed a series of model simulations as follows. In the WRF simulations, we increased AOD from 0.0 to 6.0 with an increment of 0.1 and varied the SSA from 1.0 (pure scattering) to 0.6 (strongly absorbing) (Figures 1, 3, 5, and S2). In Figure 4, the corresponding change of SSA and AOD to the reduction of BC in path 2 is mapped according to an offline optical Mie model calculation.[57] In the optical calculation, the size distribution and speciation of aerosol particles was the same as in the WRF-Chem simulations (see below). To estimate the amount of BC that is needed to be reduced in path 2, we adopted two mixing assumptions of BC particles (i.e., external mixture and core-shell mixture).[59] For the core-shell mixture, we adopted a diameter ratio of particle to BC core of 1.5–2, according to single-particle soot photometry measurements conducted in the North China Plain.[65] As a result, a ~60%–70% reduction of BC (~7%–10% reduction of AOD) would be needed, corresponding to an increase of SSA from 0.85 to 0.94 and an increase of threshold AOD from 1.2 (path 1) to 1.8 (path 2).

In the WRF-Chem simulations, we scaled the initial aerosol profile with different factors, which corresponds to a surface $PM_{2.5}$ concentration from 0 to 700 $\mu g\ m^{-3}$ in increments of 10 $\mu g\ m^{-3}$ (Figures S3A, 3E, and S16). Initial aerosol speciation was set to SO_4^{2-}:OM:NO_3^-:NH_4^+ = 3:3:2:1 in mass concentration (here, OM is organic matter). The initial size distribution of aerosol particles was set to be 1:2:2:0 in four bins in mass concentration. For the influence of absorbing aerosols, we increased the SSA from 0.60 to 1.00 at wavelength of 533 nm in increments of 0.01 in WRF simulations (Figures 1 and S2). Angstrom exponent was set to be 1.2.[66] In the WRF-Chem simulations, SSA was calculated from aerosol composition by Mie theory.[57] The BC mass fractions were set to be 0 to 0.20 with an interval of 0.01, covering most the range of BC fractions in real situations. The corresponding SSA varies from 1 to 0.63. Emissions of aerosols were set to zero in the WRF-Chem base case simulations but were included in the extended cases (see below).

Extended cases

To complement the results from the base case simulations, we studied a series of extended cases with different meteorological conditions, aerosol properties (concentration, SSA, and vertical distribution), emissions, and extra sensible heat, as well as a different boundary layer scheme.

Solar zenith angles

Incoming solar radiation can influence the PBL development. Different incoming solar radiation was tested by changing solar zenith angles. As shown in Figure S3B, 62.9°, 57.8°, 48.1°, 36.2°, 25.3°, 18.1°, and 17.0° were adopted in different cases, representing the solar zenith angle of the first day of January to July in Beijing.

Aerosol vertical distribution

In the WRF simulations, we designed the following scenarios to study the effects of different vertical profiles of aerosols, including three scenarios of uniformly distributed aerosols within the lower 230, 340, 460, and 520 m (Figure S4); a scenario of non-uniformly distributed aerosols (profile shown in Figure S3H); and a scenario of one elevated aerosol layer at ~2,000 m, mimicking a light-absorbing plume (Figure S2F).

Emissions

In the WRF-Chem simulations, we studied the effects of emission intensities by increasing the emission rate of $PM_{2.5}$ from 0 to 21 t km^{-2} $year^{-1}$ (i.e., 0, 0.42, 1.05, 2.1, 4.2, 10.5, and 21 t km^{-2} $year^{-1}$) (Figure S3C), covering the emission intensity of primary $PM_{2.5}$ in Beijing-Tianjin-Hebei region (1.2 to 17.5 t km^{-2} $year^{-1}$).[67] The $PM_{2.5}$ was set to be emitted to the surface layer with a constant rate (i.e., 0, 0.96, 2.4, 4.8, 9.6, 24, and 48 $\mu g\ m^{-3}$ $hour^{-1}$ $PM_{2.5}$ in surface layer).

Meteorological conditions

Besides the case of January 11, 2013 in Beijing, we have also performed simulations for other days and locations with corresponding initial meteorological conditions based on sounding data. There are 75 cases corresponding to target days from January 1 to January 25, 2013 and cities of Beijing, Zhengzhou (34.8°N, 113.7°E), and Nanjing (32.1°N, 118.8°E). Besides, to compare with multi-year observations of PBL height response to AOD, we have also performed simulations in Beijing for the winter season (December, January, and February) from December 2016 to February 2018. Consistent with the base case, we first simulated H_{max} at AOD = 0 under different meteorological conditions and then set the aerosol layer height as 75% of the simulated H_{max} (Figure S3A). For all 75 cases, SSA was set to be 0.85.

Note that, in the base case, the initial condition of soil for Beijing was extracted from the inner domain (9-km horizontal resolution) of the nested 3D WRF model simulation, which did not cover Zhengzhou and Nanjing. To compare the three cities here, we extracted the initial conditions of soil from the outer domain (81-km horizontal resolution), which covered all three locations. Therefore, the threshold AOD calculated for Beijing on January 11, 2013, in the extended case is slightly different than that in the base case.

Extra sensible heat

Based on the base case of AOD = 1.3 and SSA = 0.85, the sensible heat flux was set to be 1.5 times that of the sensible heat flux calculated by the model at each time step to test the influence of extra sensible heat on the PBL evolution.

Boundary layer scheme

Besides ACM2, we also tested our base case (SSA = 0.85) with the Yonsei University (YSU) PBL scheme[68] (Figures S7B) and the Mellor-Yamada-Janjic (MYJ) PBL scheme[69] (Figures S7C). The MYJ PBL scheme uses 1.5-order turbulence closure. The PBL heights in the MYJ scheme depend on the buoyancy, shear of the driving flow, and the turbulent kinetic energy (TKE).

SUPPLEMENTAL INFORMATION

Supplemental information can be found online at https://doi.org/10.1016/j.oneear.2023.05.010.

ACKNOWLEDGMENTS

This study was supported by the Max Planck Society (MPG). Y.C. would also like to acknowledge the Minerva Program of MPG.

AUTHOR CONTRIBUTIONS

Y.C. conceived and led the study. J.D.W. performed the simulation. J.D.W., Y.C., and H.S. analyzed the data and interpretated the results. C.W. supported the model configuration and simulation. G.Z. and J.P.W. supported data analyses and visualization. T.S., Z.L., C.C.L., and C.L. provided observations of PBL height. U.P., M.O.A., J.P., and A.D. discussed the results and commented on the manuscript. Y.C., H.S., and J.D.W. wrote the manuscript with inputs from all co-authors.

DECLARATION OF INTERESTS

The authors declare no competing interests.

INCLUSION AND DIVERSITY

We support inclusive, diverse, and equitable conduct of research.

Received: June 13, 2022
Revised: February 14, 2023
Accepted: May 10, 2023
Published: June 1, 2023

REFERENCES

1. Lelieveld, J., Evans, J.S., Fnais, M., Giannadaki, D., and Pozzer, A. (2015). The contribution of outdoor air pollution sources to premature mortality on a global scale. Nature *525*, 367–371. https://doi.org/10.1038/nature15371.
2. Zheng, G.J., Duan, F.K., Su, H., Ma, Y.L., Cheng, Y., Zheng, B., Zhang, Q., Huang, T., Kimoto, T., Chang, D., et al. (2015). Exploring the severe winter haze in Beijing: the impact of synoptic weather, regional transport and heterogeneous reactions. Atmos. Chem. Phys. *15*, 2969–2983. https://doi.org/10.5194/acp-15-2969-2015.
3. Cheng, Y., Zheng, G., Wei, C., Mu, Q., Zheng, B., Wang, Z., Gao, M., Zhang, Q., He, K., Carmichael, G., et al. (2016). Reactive nitrogen chemistry in aerosol water as a source of sulfate during haze events in China. Sci. Adv. *2*, e1601530. https://doi.org/10.1126/sciadv.1601530.
4. Wang, G., Zhang, R., Gomez, M.E., Yang, L., Levy Zamora, M., Hu, M., Lin, Y., Peng, J., Guo, S., Meng, J., et al. (2016). Persistent sulfate formation from London Fog to Chinese haze. Proc. Natl. Acad. Sci. USA *113*, 13630–13635. https://doi.org/10.1073/pnas.1616540113.
5. Ramanathan, V., Crutzen, P.J., Kiehl, J.T., and Rosenfeld, D. (2001). Aerosols, climate, and the hydrological cycle. Science *294*, 2119–2124. https://doi.org/10.1126/science.1064034.
6. Wilcox, E.M., Thomas, R.M., Praveen, P.S., Pistone, K., Bender, F.A.-M., and Ramanathan, V. (2016). Black carbon solar absorption suppresses turbulence in the atmospheric boundary layer. Proc. Natl. Acad. Sci. USA *113*, 11794–11799. https://doi.org/10.1073/pnas.1525746113.
7. Podgorny, I.A., Conant, W., Ramanathan, V., and Satheesh, S.K. (2000). Aerosol modulation of atmospheric and surface solar heating over the tropical Indian Ocean. Tellus B *52*, 947–958. https://doi.org/10.1034/j.1600-0889.2000.d01-4.x.
8. Crutzen, P.J., and Birks, J.W. (1982). The atmosphere after a nuclear war: twilight at noon. Ambio *11*, 114–125.
9. Rahimi, S., Liu, X., Wu, C., Lau, W.K., Brown, H., Wu, M., and Qian, Y. (2019). Quantifying snow darkening and atmospheric radiative effects of black carbon and dust on the South Asian monsoon and hydrological cycle: experiments using variable-resolution CESM. Atmos. Chem. Phys. *19*, 12025–12049. https://doi.org/10.5194/acp-19-12025-2019.
10. Wei, L., Lu, Z., Wang, Y., Liu, X., Wang, W., Wu, C., Zhao, X., Rahimi, S., Xia, W., and Jiang, Y. (2022). Black carbon-climate interactions regulate dust burdens over India revealed during COVID-19. Nat. Commun. *13*, 1839. https://doi.org/10.1038/s41467-022-29468-1.
11. Lau, K.M., Kim, M.K., and Kim, K.M. (2006). Asian summer monsoon anomalies induced by aerosol direct forcing: the role of the Tibetan Plateau. Clim. Dyn. *26*, 855–864. https://doi.org/10.1007/s00382-006-0114-z.
12. Yang, Y., Smith, S.J., Wang, H., Lou, S., and Rasch, P.J. (2019). Impact of anthropogenic emission injection height uncertainty on global sulfur dioxide and aerosol distribution. J. Geophys. Res. Atmos. *124*, 4812–4826. https://doi.org/10.1029/2018JD030001.
13. Jacobson, M.Z. (2001). Strong radiative heating due to the mixing state of black carbon in atmospheric aerosols. Nature *409*, 695–697. https://doi.org/10.1038/35055518.
14. Andreae, M.O. (2001). The dark side of aerosols. Nature *409*, 671–672. https://doi.org/10.1038/35055640.
15. Bond, T.C., Doherty, S.J., Fahey, D.W., Forster, P.M., Berntsen, T., DeAngelo, B.J., Flanner, M.G., Ghan, S., Kärcher, B., Koch, D., et al. (2013). Bounding the role of black carbon in the climate system: a scientific assessment. J. Geophys. Res. Atmos. *118*, 5380–5552. https://doi.org/10.1002/jgrd.50171.
16. Ackerman, T.P. (1977). A model of the effect of aerosols on urban climates with particular applications to the Los Angeles Basin. J. Atmos. Sci. *34*, 531–547. https://doi.org/10.1175/1520-0469.
17. Lenschow, D.H. (1986). Probing the Atmospheric Boundary Layer (Amer Meteorological Society).
18. Wendisch, M., Hellmuth, O., Ansmann, A., Heintzenberg, J., Engelmann, R., Althausen, D., Eichler, H., Müller, D., Hu, M., Zhang, Y., et al. (2008). Radiative and dynamic effects of absorbing aerosol particles over the Pearl River Delta, China. Atmos. Environ. *42*, 6405–6416. https://doi.org/10.1016/j.atmosenv.2008.02.033.
19. Ding, A.J., Huang, X., Nie, W., Sun, J.N., Kerminen, V.-M., Petäjä, T., Su, H., Cheng, Y.F., Yang, X.-Q., Wang, M.H., et al. (2016). Enhanced haze pollution by black carbon in megacities in China. Geophys. Res. Lett. *43*, 2873–2879. https://doi.org/10.1002/2016GL067745.
20. Huang, X., Wang, Z., and Ding, A. (2018). Impact of aerosol-PBL interaction on haze pollution: multiyear observational evidences in North China. Geophys. Res. Lett. *45*, 8596–8603. https://doi.org/10.1029/2018GL079239.
21. Dickerson, R.R., Kondragunta, S., Stenchikov, G., Civerolo, K.L., Doddridge, B.G., and Holben, B.N. (1997). The Impact of aerosols on solar ultraviolet radiation and photochemical smog. Science *278*, 827–830. https://doi.org/10.1126/science.278.5339.827.
22. Xing, J., Wang, J., Mathur, R., Pleim, J., Wang, S., Hogrefe, C., Gan, C.-M., Wong, D.C., and Hao, J. (2016). Unexpected benefits of reducing aerosol cooling effects. Environ. Sci. Technol. *50*, 7527–7534. https://doi.org/10.1021/acs.est.6b00767.
23. Wong, D.C., Pleim, J., Mathur, R., Binkowski, F., Otte, T., Gilliam, R., Pouliot, G., Xiu, A., Young, J.O., and Kang, D. (2012). WRF-CMAQ two-way coupled system with aerosol feedback: software development and

preliminary results. Geosci. Model Dev. (GMD) *5*, 299–312. https://doi.org/10.5194/gmd-5-299-2012.

24. Liu, C., Huang, J., Fedorovich, E., Hu, X.-M., Wang, Y., and Lee, X. (2018). Impact of aerosol shortwave radiative heating on the entrainment in atmospheric convective boundary layer: a large-eddy simulation study. J. Atmos. Sci. *9*, 347–799. https://doi.org/10.3390/atmos9090347.
25. Liu, C., Huang, J., Fedorovich, E., Hu, X.-M., Wang, Y., and Lee, X. (2018). The effect of aerosol radiative heating on turbulence statistics and spectra in the atmospheric convective boundary layer: a large-eddy simulation study. Atmosphere *9*, 347. https://doi.org/10.3390/atmos9090347.
26. Yu, H., Liu, S., and Dickinson, R.E. (2002). Radiative effects of aerosols on the evolution of the atmospheric boundary layer. J. Geophys. Res-Atmos. *107*, AAC 3-1–AAC 3-14. https://doi.org/10.1029/2001JD000754.
27. Rudich, Y., Sagi, A., and Rosenfeld, D. (2003). Influence of the Kuwait oil fires plume (1991) on the microphysical development of clouds. J. Geophys. Res. *108*, 4478. https://doi.org/10.1029/2003jd003472.
28. Barbaro, E., Vilà-Guerau de Arellano, J., Krol, M.C., and Holtslag, A.A.M. (2013). Impacts of aerosol shortwave radiation absorption on the dynamics of an idealized convective atmospheric boundary layer. BoundLay. Meteorol. *148*, 31–49. https://doi.org/10.1007/s10546-013-9800-7.
29. Li, Z., Guo, J., Ding, A., Liao, H., Liu, J., Sun, Y., Wang, T., Xue, H., Zhang, H., and Zhu, B. (2017). Aerosol and boundary-layer interactions and impact on air quality. Natl. Sci. Rev. *4*, 810–833. https://doi.org/10.1093/nsr/nwx117.
30. Jacobson, M.Z. (1998). Studying the effects of aerosols on vertical photolysis rate coefficient and temperature profiles over an urban airshed. J. Geophys. Res. *103*, 10593–10604. https://doi.org/10.1029/98jd00287.
31. Tie, X., Huang, R.-J., Cao, J., Zhang, Q., Cheng, Y., Su, H., Chang, D., Pöschl, U., Hoffmann, T., Dusek, U., et al. (2017). Severe pollution in China amplified by atmospheric moisture. Sci. Rep. *7*, 15760. https://doi.org/10.1038/s41598-017-15909-1.
32. Twomey, S. (1977). The influence of pollution on the shortwave albedo of clouds. J. Atmos. Sci. *34*, 1149–1152. https://doi.org/10.1175/1520-0469(1977)034<1149:tiopot>2.0.co;2.
33. Ding, K., Huang, X., Ding, A., Wang, M., Su, H., Kerminen, V.-M., Petäjä, T., Tan, Z., Wang, Z., Zhou, D., et al. (2021). Aerosol-boundary-layer-monsoon interactions amplify semi-direct effect of biomass smoke on low cloud formation in Southeast Asia. Nat. Commun. *12*, 6416. https://doi.org/10.1038/s41467-021-26728-4.
34. Xie, Y., Wang, Y., Zhang, K., Dong, W., Lv, B., and Bai, Y. (2015). Daily estimation of ground-level $PM_{2.5}$ concentrations over beijing using 3 km resolution MODIS AOD. Environ. Sci. Technol. *49*, 12280–12288. https://doi.org/10.1021/acs.est.5b01413.
35. Zheng, C., Zhao, C., Zhu, Y., Wang, Y., Shi, X., Wu, X., Chen, T., Wu, F., and Qiu, Y. (2017). Analysis of influential factors for the relationship between PM2.5 and AOD in Beijing. Atmos. Chem. Phys. *17*, 13473–13489. https://doi.org/10.5194/acp-17-13473-2017.
36. Radke, L.F., Lyons, J.H., Hobbs, P.V., and Weiss, R.E. (1990). Smokes from the burning of aviation fuel and their self-lofting by solar heating. J. Geophys. Res. *95*, 14071–14076. https://doi.org/10.1029/JD095iD09p14071.
37. Boers, R., de Laat, A.T., Stein Zweers, D.C., and Dirksen, R.J. (2010). Lifting potential of solar-heated aerosol layers. Geophys. Res. Lett. *37*. https://doi.org/10.1029/2010GL045171.
38. de Laat, A.T.J., Stein Zweers, D.C., Boers, R., and Tuinder, O.N.E. (2012). A solar escalator: observational evidence of the self-lifting of smoke and aerosols by absorption of solar radiation in the February 2009 Australian Black Saturday plume. J. Geophys. Res. *117*. https://doi.org/10.1029/2011jd017016.
39. Lelieveld, J., Klingmüller, K., Pozzer, A., Burnett, R.T., Haines, A., and Ramanathan, V. (2019). Effects of fossil fuel and total anthropogenic emission removal on public health and climate. Proc. Natl. Acad. Sci. USA *116*, 7192–7197. https://doi.org/10.1073/pnas.1819989116.
40. Liu, D., Zhao, D., Xie, Z., Yu, C., Chen, Y., Tian, P., Ding, S., Hu, K., Lowe, D., Liu, Q., et al. (2019). Enhanced heating rate of black carbon above the planetary boundary layer over megacities in summertime. Environ. Res. Lett. *14*, 124003. https://doi.org/10.1088/1748-9326/ab4872.
41. Liu, D., Hu, K., Zhao, D., Ding, S., Wu, Y., Zhou, C., Yu, C., Tian, P., Liu, Q., Bi, K., et al. (2020). Efficient vertical transport of black carbon in the planetary boundary layer. Geophys. Res. Lett. *47*, e2020GL088858. https://doi.org/10.1029/2020GL088858.
42. Ramanathan, V., and Carmichael, G. (2008). Global and regional climate changes due to black carbon. Nat. Geosci. *1*, 221–227. https://doi.org/10.1038/ngeo156.
43. Malone, R.C., Auer, L.H., Glatzmaier, G.A., Wood, M.C., and Toon, O.B. (1986). Nuclear winter: three-dimensional simulations including interactive transport, scavenging, and solar heating of smoke. J. Geophys. Res. *91*, 1039–1053. https://doi.org/10.1029/JD091iD01p01039.
44. Andreae, M.O., and Ramanathan, V. (2013). Climate's dark forcings. Science *340*, 280–281. https://doi.org/10.1126/science.1235731.
45. Shindell, D., Kuylenstierna, J.C.I., Vignati, E., van Dingenen, R., Amann, M., Klimont, Z., Anenberg, S.C., Muller, N., Janssens-Maenhout, G., Raes, F., et al. (2012). Simultaneously mitigating near-term climate change and improving human health and food security. Science *335*, 183–189. https://doi.org/10.1126/science.1210026.
46. Cai, W., Li, K., Liao, H., Wang, H., and Wu, L. (2017). Weather conditions conducive to Beijing severe haze more frequent under climate change. Nat. Clim. Change *7*, 257–262. https://doi.org/10.1038/nclimate3249.
47. Li, J., Hao, X., Liao, H., Wang, Y., Cai, W., Li, K., Yue, X., Yang, Y., Chen, H., Mao, Y., et al. (2022). Winter particulate pollution severity in North China driven by atmospheric teleconnections. Nat. Geosci. *15*, 349–355. https://doi.org/10.1038/s41561-022-00933-2.
48. Yang, Y., Zhou, Y., Li, K., Wang, H., Ren, L., Zeng, L., Li, H., Wang, P., Li, B., and Liao, H. (2021). Atmospheric circulation patterns conducive to severe haze in eastern China have shifted under climate change. Geophys. Res. Lett. *48*. https://doi.org/10.1029/2021GL095011.
49. Huang, X., Ding, K., Liu, J., Wang, Z., Tang, R., Xue, L., Wang, H., Zhang, Q., Tan, Z.-M., Fu, C., et al. (2023). Smoke-weather interaction affects extreme wildfires in diverse coastal regions. Science *379*, 457–461. https://doi.org/10.1126/science.add9843.
50. Grell, G.A., Peckham, S.E., Schmitz, R., McKeen, S.A., Frost, G., Skamarock, W.C., and Eder, B. (2005). Fully coupled "online" chemistry within the WRF model. Atmos. Environ. X. *39*, 6957–6975. https://doi.org/10.1016/j.atmosenv.2005.04.027.
51. Iacono, M.J., Delamere, J.S., Mlawer, E.J., Shephard, M.W., Clough, S.A., and Collins, W.D. (2008). Radiative forcing by long-lived greenhouse gases: calculations with the AER radiative transfer models. J. Geophys. Res. *113*, D13103. https://doi.org/10.1029/2008JD009944.
52. Morrison, H., and Gettelman, A. (2008). A new two-moment bulk stratiform cloud microphysics scheme in the community atmosphere model, version 3 (CAM3). Part I: description and numerical tests. J. Clim. *21*, 3642–3659. https://doi.org/10.1175/2008JCLI2105.1.
53. Chen, F., Mitchell, K., Schaake, J., Xue, Y., Pan, H.-L., Koren, V., Duan, Q.Y., Ek, M., and Betts, A. (1996). Modeling of land surface evaporation by four schemes and comparison with FIFE observations. J. Geophys. Res. *101*, 7251–7268. https://doi.org/10.1029/95JD02165.
54. Pleim, J.E. (2007). A combined local and nonlocal closure model for the atmospheric boundary layer. Part I: model description and testing. J. Appl. Meteorol. Climatol. *46*, 1383–1395. https://doi.org/10.1175/JAM2539.1.
55. Hauglustaine, D.A., Brasseur, G.P., Walters, S., Rasch, P.J., Müller, J.F., Emmons, L.K., and Carroll, M.A. (1998). MOZART, a global chemical transport model for ozone and related chemical tracers: 1. Model description. J. Geophys. Res. *103*, 28291–28335. https://doi.org/10.1029/98JD02398.
56. Zaveri, R.A., and Peters, L.K. (1999). A new lumped structure photochemical mechanism for large-scale applications. J. Geophys. Res. *104*, 30387–30415. https://doi.org/10.1029/1999jd900876.

57. Bohren, C.F., and Huffman, D.R. (1983). Absorption and scattering of light by small particles. Wiley Science Paperback Series, *7* (John Wiley & Sons). 7.5.

58. National Centers for Environmental Prediction/National Weather Service/NOAA/U.S. (2000). Department of commerce: NCEP FNL operational model global tropospheric analyses, continuing from July 1999. https://doi.org/10.5065/D6M043C6.

59. Su, T., Li, Z., Li, C., Li, J., Han, W., Shen, C., Tan, W., Wei, J., and Guo, J. (2020). The significant impact of aerosol vertical structure on lower atmosphere stability and its critical role in aerosol–planetary boundary layer (PBL) interactions. Atmos. Chem. Phys. *20*, 3713–3724. https://doi.org/10.5194/acp-20-3713-2020.

60. Zheng, B., Zhang, Q., Zhang, Y., He, K.B., Wang, K., Zheng, G.J., Duan, F.K., Ma, Y.L., and Kimoto, T. (2015). Heterogeneous chemistry: a mechanism missing in current models to explain secondary inorganic aerosol formation during the January 2013 haze episode in North China. Atmos. Chem. Phys. *15*, 2031–2049. https://doi.org/10.5194/acp-15-2031-2015.

61. Zhang, Y.L., and Cao, F. (2015). Fine particulate matter ($PM_{2.5}$) in China at a city level. Sci. Rep. *5*, 14884. https://doi.org/10.1038/srep14884.

62. Sun, Y., Jiang, Q., Wang, Z., Fu, P., Li, J., Yang, T., and Yin, Y. (2014). Investigation of the sources and evolution processes of severe haze pollution in Beijing in January 2013. J. Geophys. Res. Atmos. *119*, 4380–4398. https://doi.org/10.1002/2014JD021641.

63. Liao, H., Chang, W., and Yang, Y. (2015). Climatic effects of air pollutants over China: a review. Adv. Atmos. Sci. *32*, 115–139. https://doi.org/10.1007/s00376-014-0013-x.

64. Andrews, E., Sheridan, P.J., Fiebig, M., McComiskey, A., Ogren, J.A., Arnott, P., Covert, D., Elleman, R., Gasparini, R., Collins, D., et al. (2006). Comparison of methods for deriving aerosol asymmetry parameter. J. Geophys. Res. *111*, D05S04. https://doi.org/10.1029/2004JD005734.

65. Zhang, Y., Zhang, Q., Cheng, Y., Su, H., Li, H., Li, M., Zhang, X., Ding, A., and He, K. (2018). Amplification of light absorption of black carbon associated with air pollution. Atmos. Chem. Phys. *18*, 9879–9896. https://doi.org/10.5194/acp-18-9879-2018.

66. Gong, C., Xin, J., Wang, S., Wang, Y., Wang, P., Wang, L., and Li, P. (2014). The aerosol direct radiative forcing over the Beijing metropolitan area from 2004 to 2011. J. Aerosol Sci. *69*, 62–70. https://doi.org/10.1016/j.jaerosci.2013.12.007.

67. Zhao, B., Wang, S., Wang, J., Fu, J.S., Liu, T., Xu, J., Fu, X., and Hao, J. (2013). Impact of national NO_x and SO_2 control policies on particulae matter pollution in China. Atmos. Environ. *77*, 453–463. https://doi.org/10.1016/j.atmosenv.2013.05.012.

68. Hong, S.Y., Noh, Y., and Dudhia, J. (2006). A new vertical diffusion package with an explicit treatment of entrainment processes. Mon. Weather Rev. *134*, 2318–2341. https://doi.org/10.1175/Mwr3199.1.

69. Mellor, G.L., and Yamada, T. (1982). Development of a turbulence closure model for geophysical fluid problems. Rev. Geophys. *20*, 851–875. https://doi.org/10.1029/RG020i004p00851.

One Earth, Volume *6*

Supplemental information

Black-carbon-induced regime transition of boundary layer development strongly amplifies severe haze

Jiandong Wang, Hang Su, Chao Wei, Guangjie Zheng, Jiaping Wang, Tianning Su, Chengcai Li, Cheng Liu, Jonathan E. Pleim, Zhanqing Li, Aijun Ding, Meinrat O. Andreae, Ulrich Pöschl, and Yafang Cheng

SUPPLEMENTAL INFORMATION

supplemental items

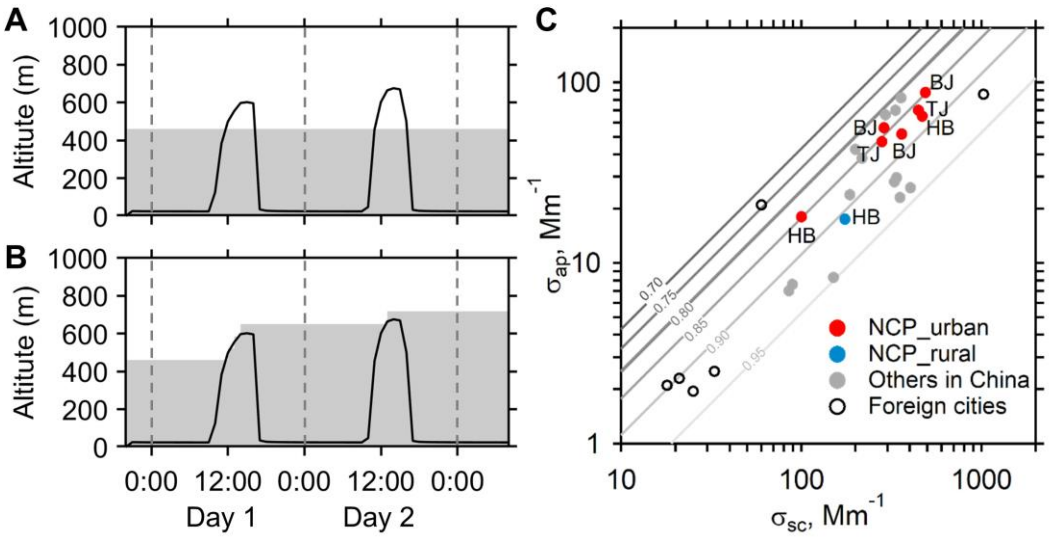

Figure S1: Illustration of base cases settings

A) WRF cases, where the aerosol vertical distribution is fixed to better illustrate the impact of aerosol on development of the planetary boundary layer (PBL). B) WRF-Chem cases, where the aerosol diffusion is taken into considerations. The black line shows PBL height without aerosol perturbation. The grey shadow shows aerosol layer height. Under initial conditions, aerosol is uniformly distributed in aerosol layers. Aerosol layer height is set to 460 m, based on a previous study[1], which is slightly lower than the max PBL height (without aerosol perturbation) in Day 1. Simulations all start at 20:00 (Beijing local time) in Day 0. C) Comparison of aerosol single scattering albedo (SSA) in different cities, including Beijing and cities in the North China Plain (NCP). Here, σ_{sc} and σ_{ap} are the aerosol scattering and absorption coefficients, respectively. BJ, SH, GZ, NJ, HK, TY, FN, US, and DE means sites in Beijing[2-3], Shanghai[4-7], Guangzhou[8-9], Nanjing[10-13], Hong Kong[14], Tongyu[15], Finland[16], United States[17-18] and Germany[19-20]. Adopted from Shen *et al.* [13]. SSA in the base case has been set to 0.85 accordingly.

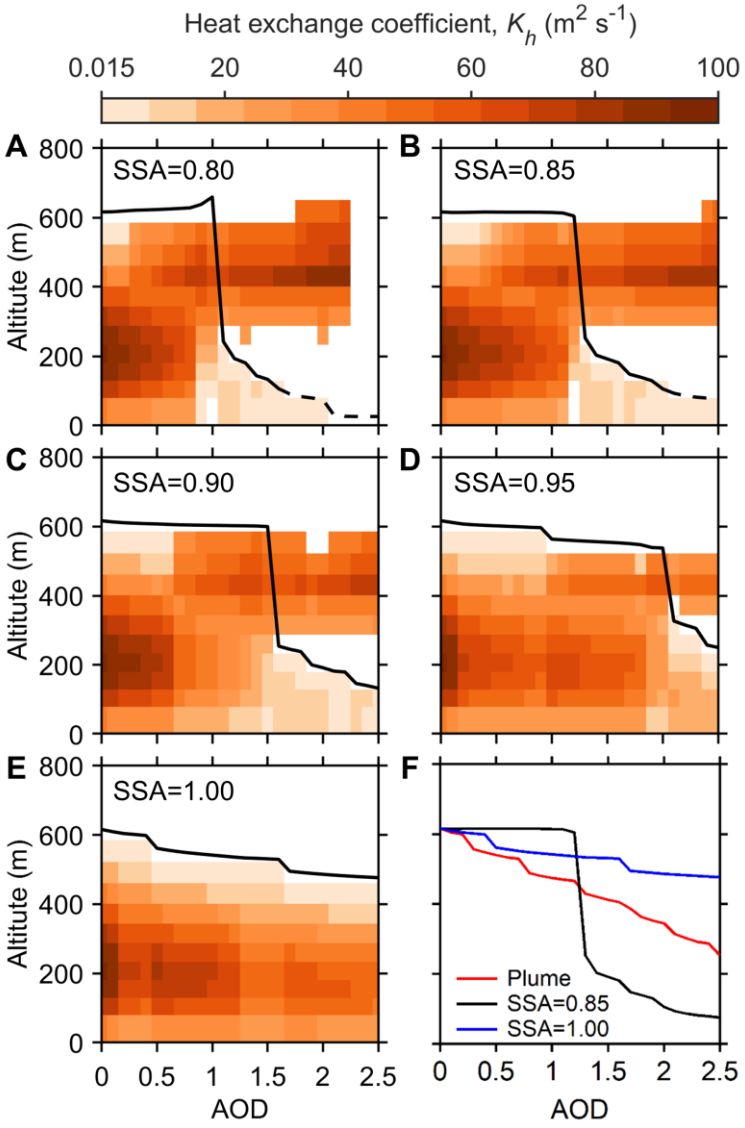

Figure S2: Impact of BC on aerosol-PBL interactions

A) WRF simulated Planetary Boundary Layer (PBL) height (black line) and vertical profile of heat exchange coefficient (K_h, colour contour) at the time of maximum PBL height, as a function of aerosol optical depth (AOD) with aerosol single scattering albedo (SSA) = 0.80. The black dashed line indicates the PBL height of the pseudo-nocturnal boundary layer, referring to the situation when sensible fluxes are nearly zero and the PBL structure is similar to the nocturnal boundary layer. The grid cells with K_h lower than 0.015 are set to white colour. B) The same as in A, but with SSA = 0.85. C) The same as in A, but with SSA = 0.90. D) The same as in A, but with SSA = 0.95. E) The same as in A, but with SSA = 1.00. F) WRF simulated PBL height as a function of AOD in the smoke plume case (SSA = 0.85) and in the uniformly distributed scenarios with SSA = 1.0 and SSA = 0.85. The results from our plume case are consistent with a previous column model study by Wang *et al.* [21].

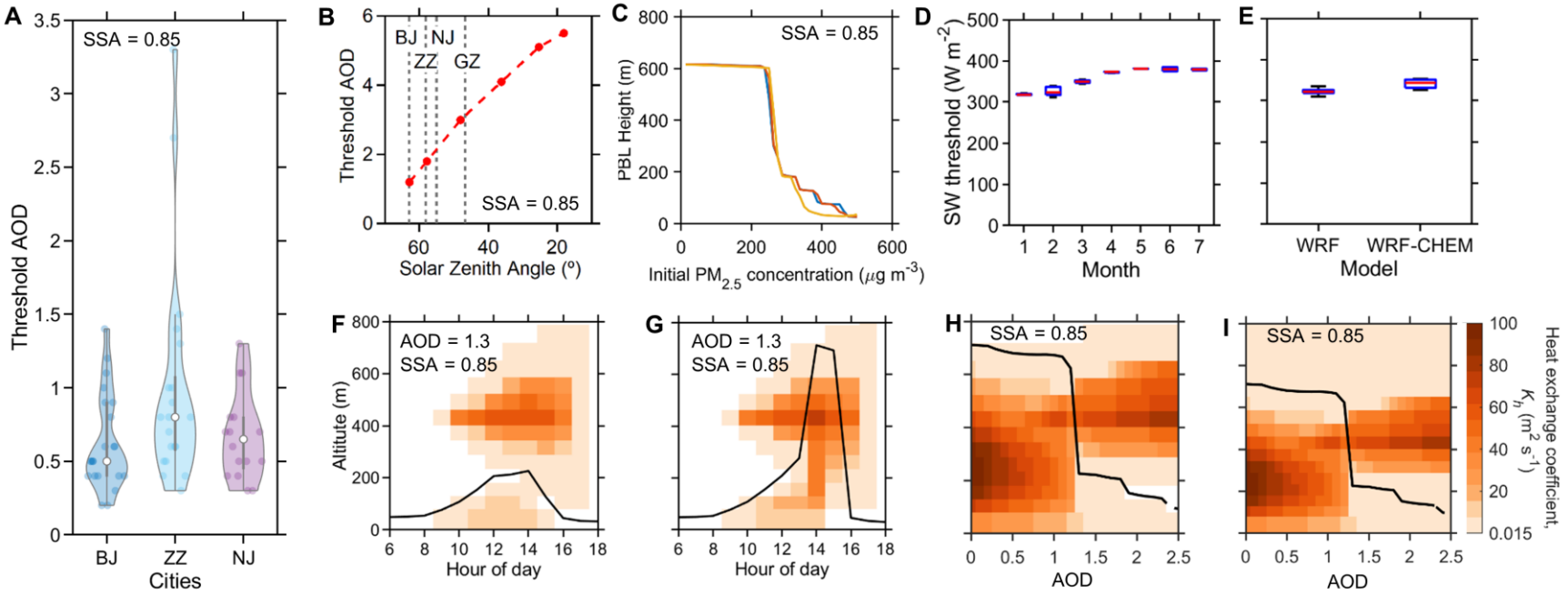

Figure S3: Threshold AOD commonly exists with presence of black carbon

A) Threshold AOD in Beijing (BJ), Zhengzhou (ZZ) and Nanjing (NJ) in January 2013. The white circles and grey bars represent median value and interquartile range, respectively. The grey lines are the 95% confidence interval and the width of the shaded area represents the frequency of occurrence. B) Threshold AOD under different solar zenith angles. Red solid circles represent solar zenith angles on the first day of January to June in BJ. The grey dashed lines show the solar zenith angles of BJ, ZZ, NJ and Guangzhou (GZ) on January 11. C) Maximum PBL height as a function of initial surface $PM_{2.5}$ concentration and different emission rates, i.e., no emission and with normal (4.2 t km^{-2} $year^{-1}$) and high (10.5 t km^{-2} $year^{-1}$) emission rates. The impact of different aerosol emission rates is not noticeable. D) Thresholds of surface shortwave (SW) solar radiations with different SSA in the base case. The central mark and the bottom and top edges of the box indicate the median and the 25th and 75th percentiles, respectively. The whiskers extend to the extreme data points. Simulations without abrupt changes of the PBL height were not included. E) Thresholds of surface SW solar radiation at different solar zenith angles. The threshold surface SW solar radiation corresponds to the energy needed to touch the bottom of the upper mixing zone, whose values vary little with different SSA and solar zenith angle. F) The same as in Fig. 2C. G) The same as in Fig. 2C and F, but with 1.5 times of extra sensitive heat. H) The same as in Fig. 1A, except that aerosol is not uniformly distributed. The fraction of ΔAOD in each layer is 0.15, 0.14, 0.13, 0.12, 0.11, 0.10, 0.09, 0.08, 0.07, and 0.01, from layer 1 near ground to layer 10, respectively. The similar abrupt change indicates that uniform vertical distribution of aerosols is not a crucial condition for the regime transition of aerosol-PBL interactions. I) The same as in Fig. 1A, but simulations with sounding measured vertical wind profile. It shows that the dependence of PBL height and AOD exhibits a pattern similar to the simulations without wind shear, i.e., still with a tipping point and two distinct regimes. Overall, the presence of wind shear does not change the generic regime of BC-induced aerosol-PBL interactions, although the threshold AOD may slightly increase.

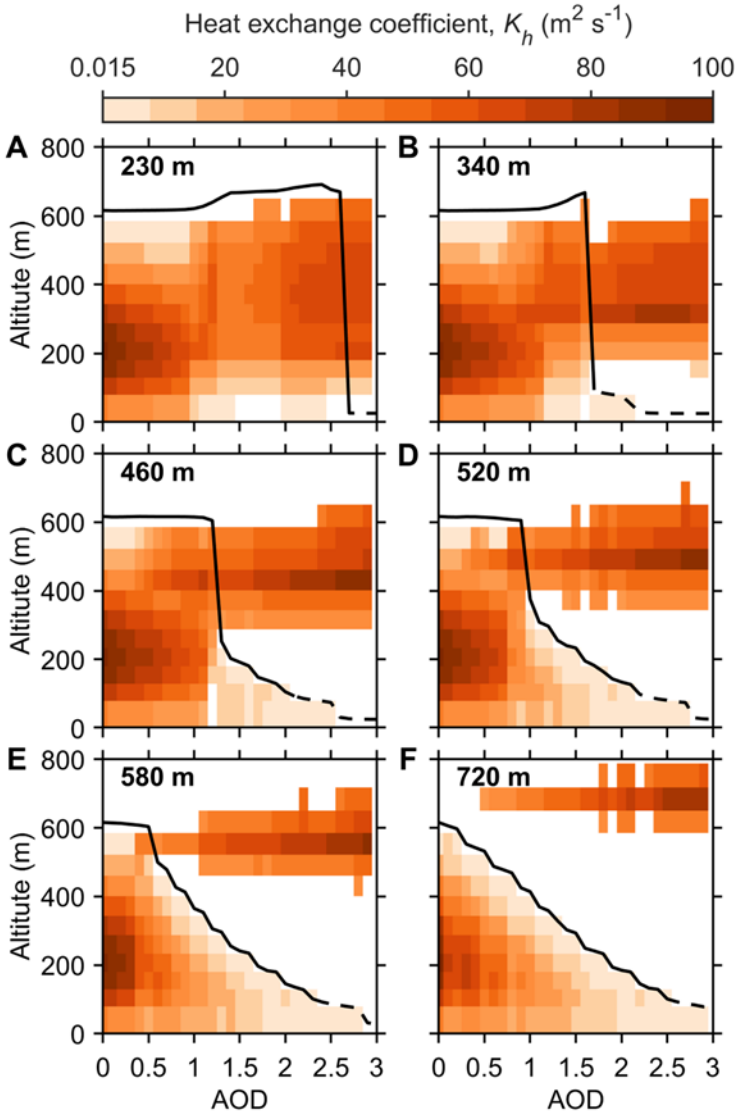

Figure S4: Impact of aerosol on PBL heights in cases with different aerosol layer top height

Similar to Fig. 1A, WRF simulated Planetary Boundary Layer (PBL) height (black line) and vertical profile of heat exchange coefficient (K_h, colour contour) at the time of maximum PBL height, as a function of aerosol optical depth (AOD) and aerosol layer top height (H_{alt}). Aerosol single scattering albedo (SSA) is set to be 0.85. The black dashed line indicates the PBL height of the pseudo-nocturnal boundary layer, referring to the situation when sensible fluxes are nearly zero and the PBL structure is similar to the nocturnal boundary layer. The grid cells with K_h lower than 0.015 are set to white colour. A) H_{alt} = 230 m. B) H_{alt} = 340 m. C) H_{alt} = 460 m. D) H_{alt} = 520 m. E) H_{alt} = 582 m. F) H_{alt} = 720 m. The abrupt decrease of the PBL height occurs at all different settings of aerosol layer top height. Threshold AOD decreases as the aerosol layer gets higher, and the impact on the reduction of PBL height during and after transitions becomes weaker as the aerosol layer gets higher.

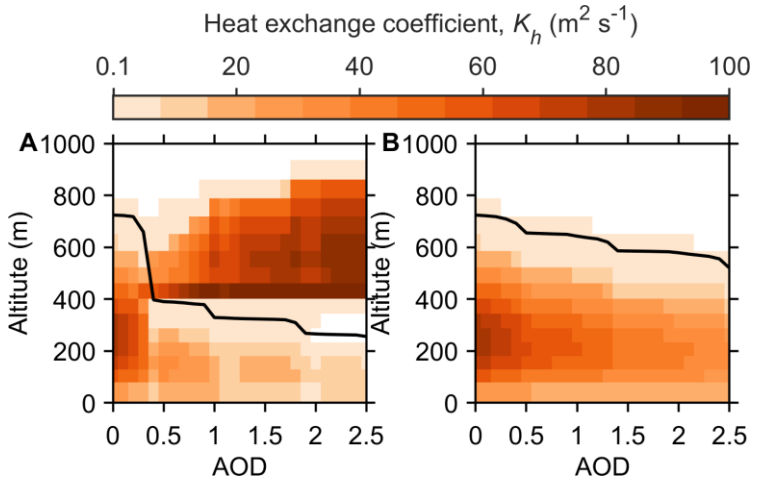

Figure S5: Impact of BC on aerosol-PBL interactions.

WRF simulated Planetary Boundary Layer (PBL) height (black line) and vertical profile of heat exchange coefficient (K_h, colour contour) at the time of maximum PBL height, as a function of aerosol optical depth (AOD) with A) SSA = 0.85 and B) SSA = 1.00. Only one layer of aerosol at around 460 m is set. The black dashed line indicates the PBL height of the pseudo-nocturnal boundary layer, referring to the situation when sensible fluxes are nearly zero and the PBL structure is similar to the nocturnal boundary layer. The grid cells with K_h lower than 0.015 are set to white colour.

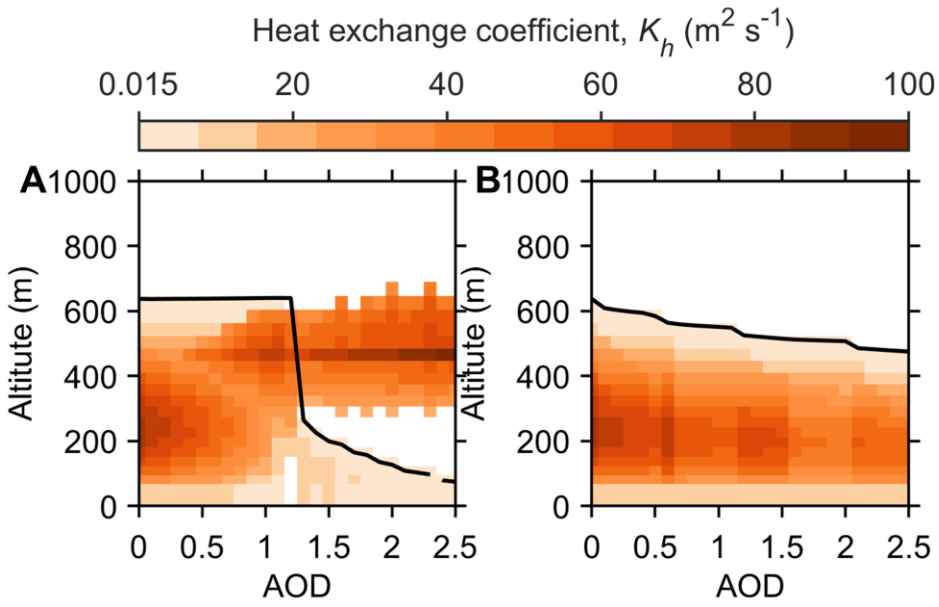

Figure S6: Impact of BC on aerosol-PBL interactions

A) and B) the same as Fig. 1A, B but with a higher vertical resolution.

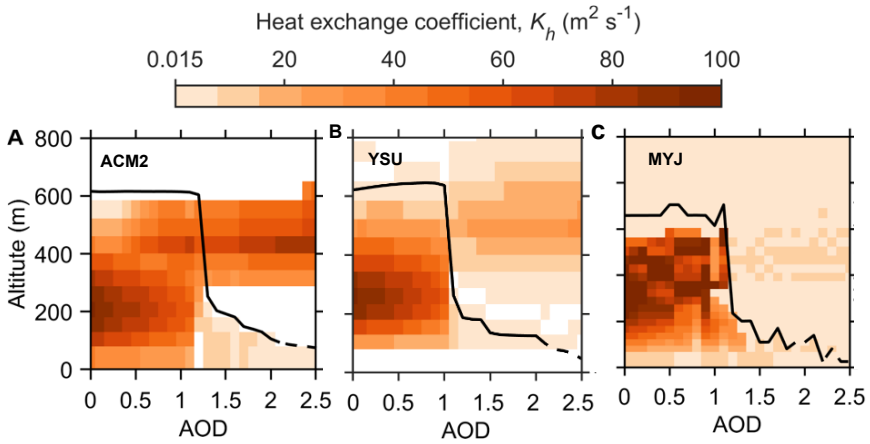

Figure S7: The comparison of results between different PBL modules.

WRF simulated maximum Planetary Boundary Layer (PBL) height (black line) and vertical profile of corresponding heat exchange coefficient (K_h, colour contour) as a function of aerosol optical depth (AOD). The aerosol single scattering albedo (SSA) is set to be 0.85. The blue dashed line and blue arrow mark the threshold AOD for a regime transition of aerosol-PBL interaction and abrupt change of the maximum PBL height in the presence of BC. The grid cells with K_h lower than 0.015 are set to white colour. A) ACM2 PBL module B) YSU PBL scheme. C) MYJ PBL scheme.

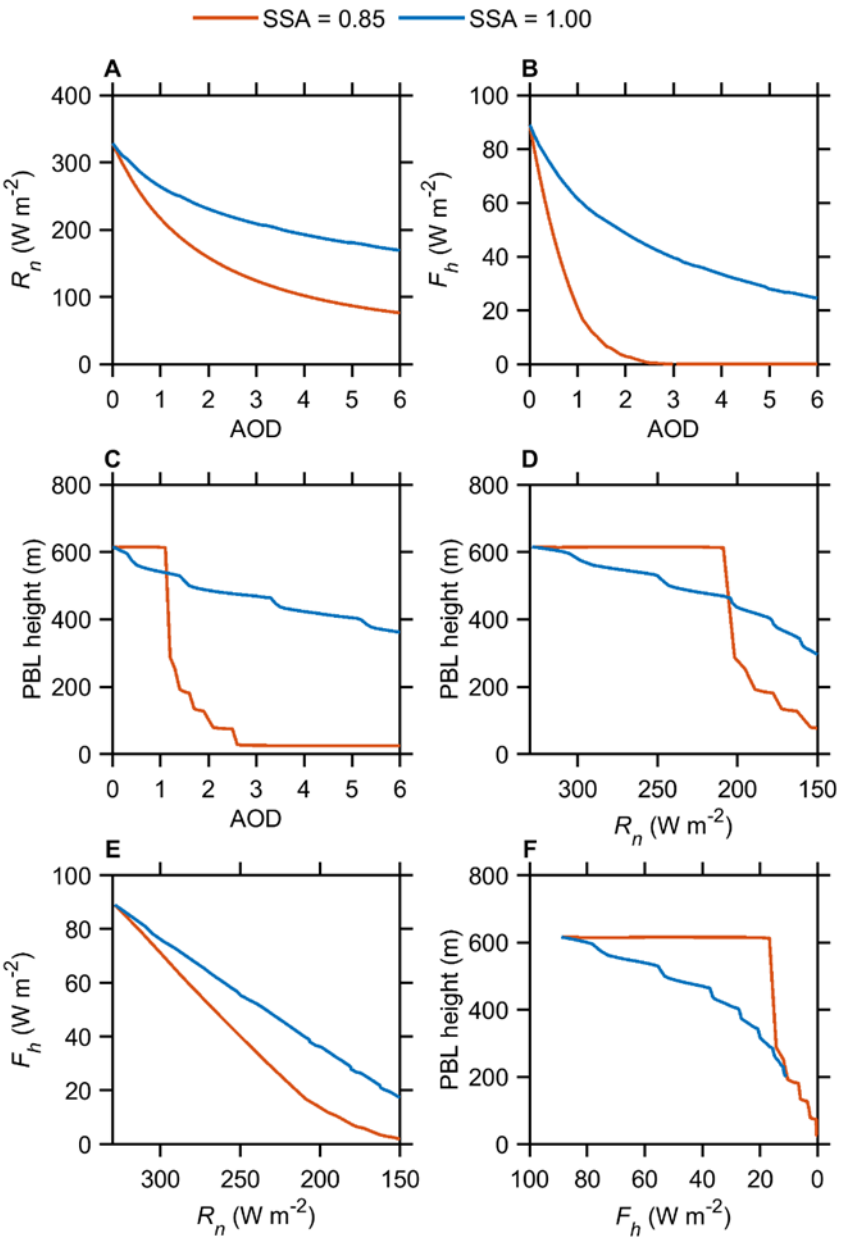

Figure S8: WRF simulated variations of net surface solar radiation and sensible heat flux with AOD and their impacts on PBL height at 14:00 under different SSA scenarios

A) Variations of net surface solar radiation (R_n) responding to AOD change. Comparing with pure scattering aerosol (SSA = 1.0), the presence of light absorbing black carbon (BC) (SSA = 0.85) leads to a smaller forward scattering to extinction ratio, and thus less solar radiation reaching the ground under the same AOD. B) Variations of sensible heat flux (F_h) responding to AOD change. C) Variations of PBL height responding to AOD change. D) The PBL height variation with R_n. E) The F_h variation with R_n. F) The PBL height variation with F_h. BC also leads to an additional heating of the atmosphere, reducing the heat fluxes as in B and E.

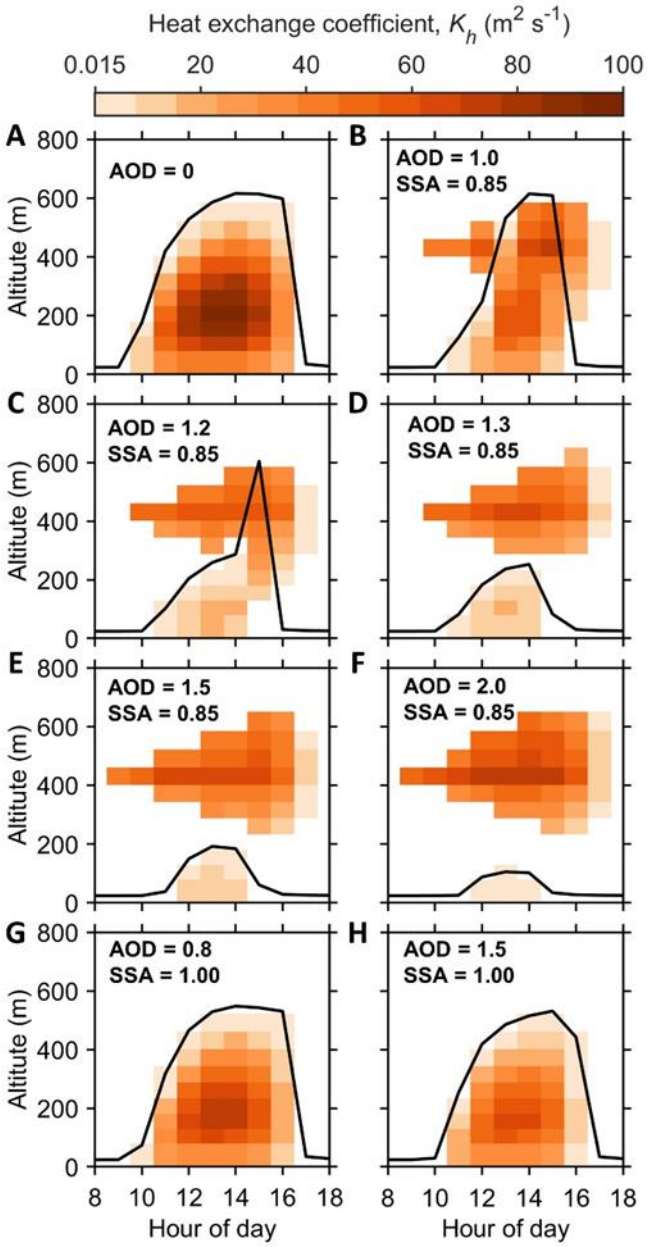

Figure S9: Coupling and decoupling of the mixing zones determines the diurnal evolution of the PBL

Similar to Fig. 2, but more scenarios are shown here. A) Diurnal variation of PBL height (black line) and vertical profile of heat exchange coefficient (K_h, colour contour) with AOD = 0.0. Grid cells with K_h lower than 0.015 are set to white colour. B) The same as in A, but with AOD = 1.0 and SSA = 0.85. C) The same as in A, but with AOD = 1.2 and SSA = 0.85. D) The same as in A, but with AOD = 1.3 and SSA = 0.85. E) The same as in A, but with AOD = 1.5 and SSA = 0.85. F) The same as in A, but with AOD = 2.0 and SSA = 0.85. G) The same as in A, but with AOD = 0.8 and SSA = 1.0. H) The same as in A, but with AOD = 1.5 and SSA = 1.0. No upper mixing zone for scenarios without BC (SSA = 1.0, as in G and H).

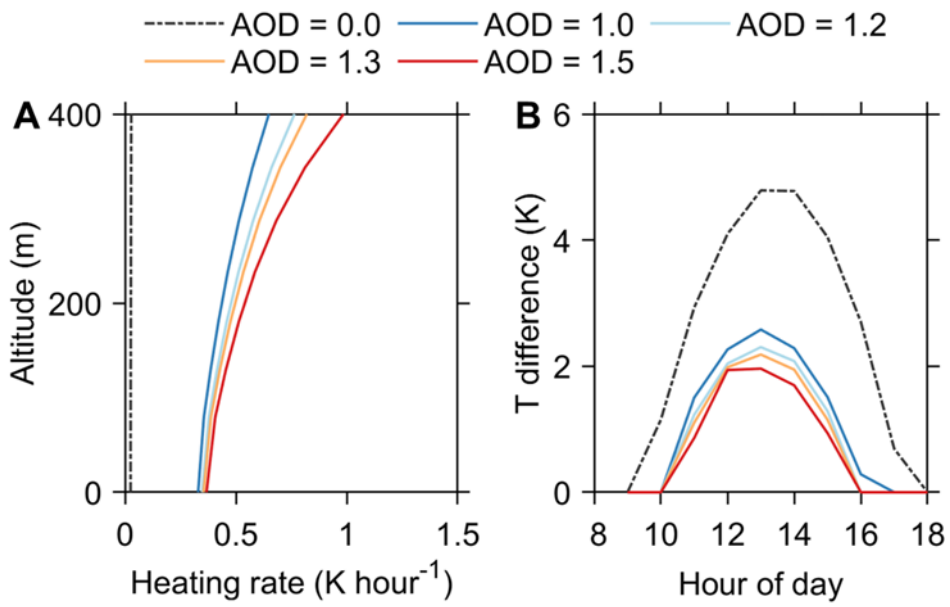

Figure S10: Aerosol induced heating rate and surface temperature difference between soil skin and 2-m air in base case

A) Vertical profiles of aerosol induced heating rate at 14:00 (local time), on January 11, 2013 with AOD = 0.0, 1.0, 1.2, 1.3 and 1.5. A gradient in the aerosol heating for uniformly distributed aerosol with higher heating rate at higher altitude. B) Diurnal variation of temperature difference between soil skin temperature and air temperature at 2 m height with the same AOD scenarios as in A. Positive values indicate the soil skin temperature is higher than that of 2-m air.

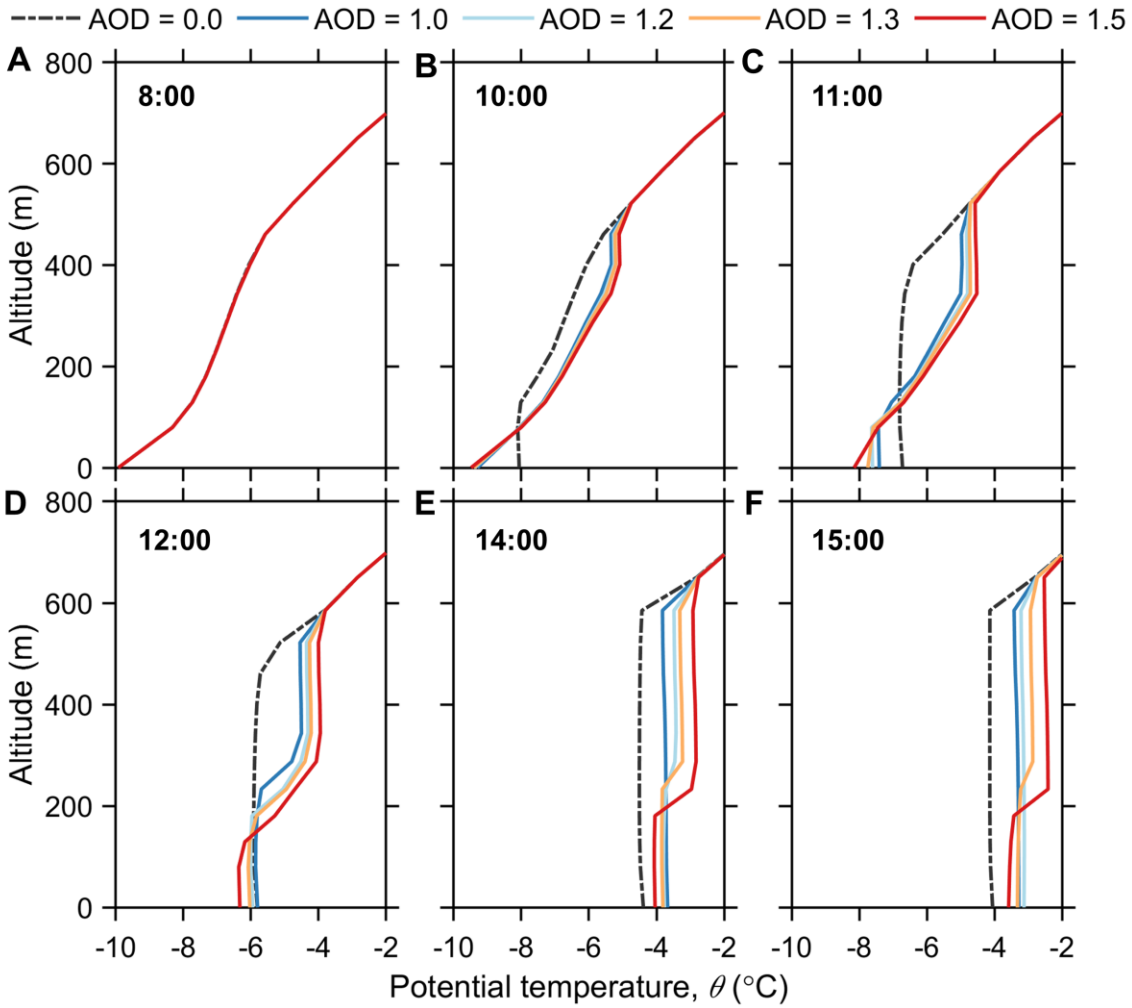

Figure S11: Evolution of vertical profile of potential temperature with different AOD in base case

A) Vertical profiles of potential temperature at 8:00. B) The same as in a, but at 10:00. C) The same as in A, but at 11:00. D) The same as in A, but at 12:00. E) The same as in A, but at 14:00. F) The same as in A, but at 15:00 local time. A strengthened inversion induced by black carbon (BC) exists in the residual layer in the morning, retarding the full development of the PBL. Scenarios with AOD below the threshold show uniform potential temperature θ around 15:00, which proves that the strong mixing effect is able to eliminate the daytime gradient and dilute air pollutants emitted at the surface by upward transport. Scenarios with AOD above the threshold present inversion at around the top of the surface zone and suppress further development of the PBL in the afternoon.

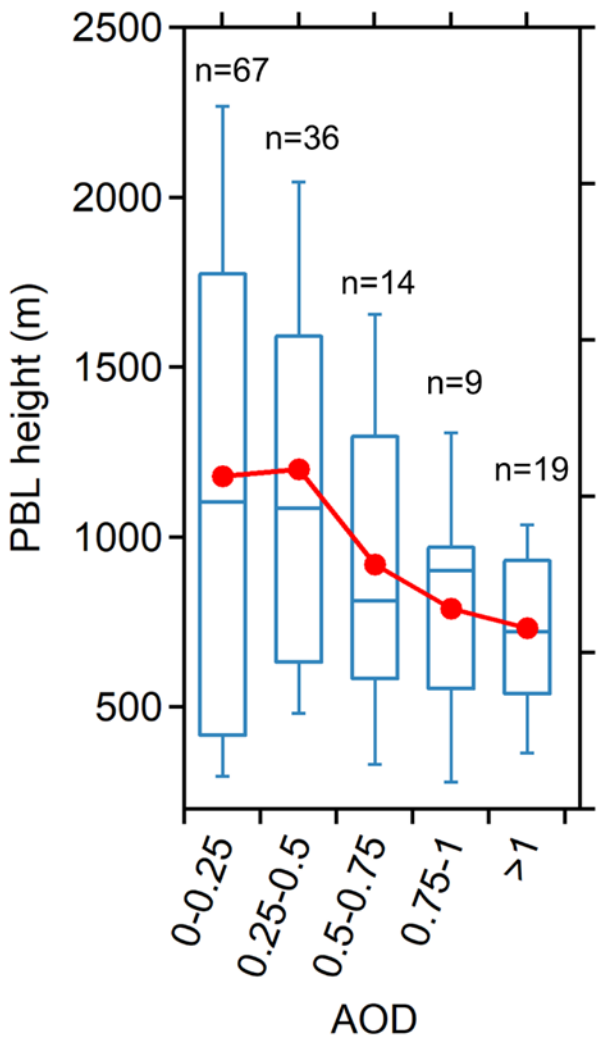

Figure S12: Observed distribution of daytime PBL heights under different AODs in the winter season in Beijing

As detailed in Su et al.[22], the daytime PBL height is derived from ground-based lidar measurements (39.99°N, 116.31°E) during 13:00-15:00 local time, and AOD data are version 3 Level 1.5 product from the AERONET site (40°N, 116.38°E). The winter season data include measurement data in December, January, and February from December 2016 to February 2018.

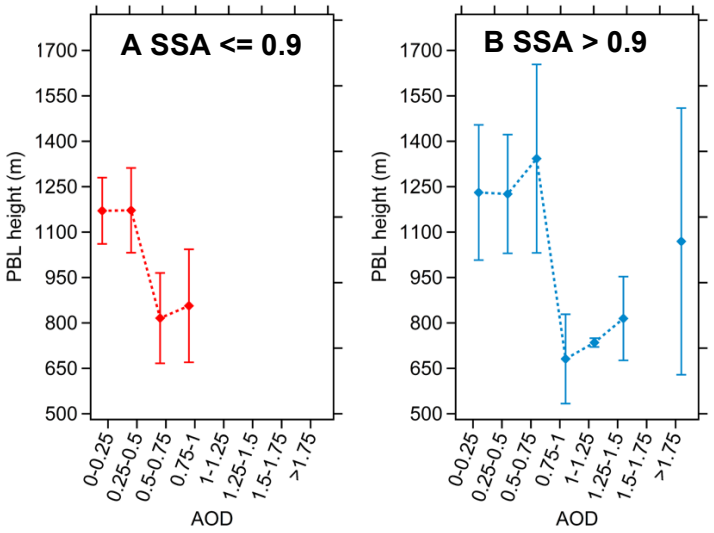

Figure S13: Observed average PBL height at noon versus corresponding AOD in winter Beijing

As detailed in Su et al.[22], the daytime PBL height is derived from ground-based lidar measurements (39.99°N, 116.31°E) during 13:00-15:00 local time, and AOD data are version 3 Level 1.5 product from the AERONET site (40°N, 116.38°E). The winter season data include measurement data in December, January, and February from December 2016 to February 2018. Diamonds represent the mean value, and the whiskers show the standard error of mean. A) days with daily average surface SSA <= 0.9. B) days with daily average surface SSA > 0.9.

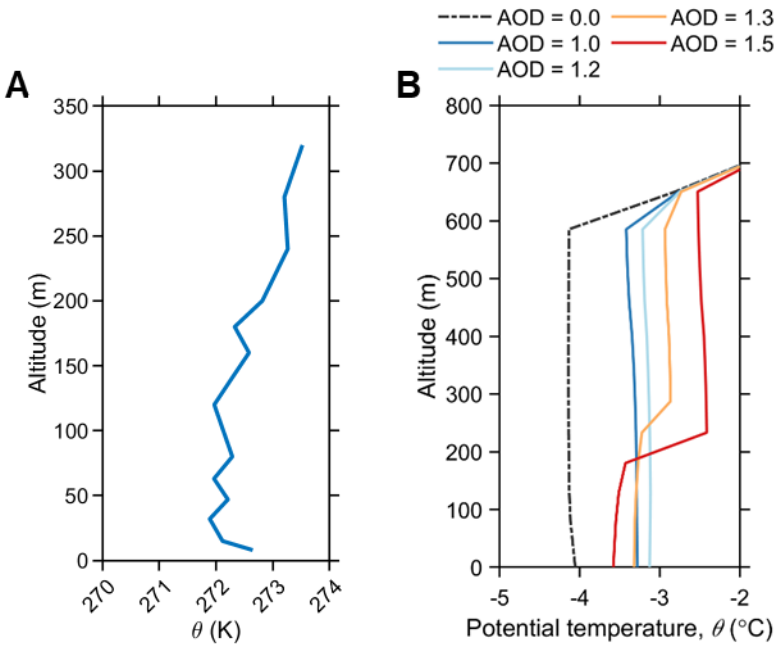

Fig. S14: Observed and simulated vertical profiles of potential temperature.
A) Observed vertical profile of potential temperature was adopted from a 325 m meteorological tower in Beijing, detailed in Sun et al, 2014[1]. B) Simulated vertical profiles of potential temperature.

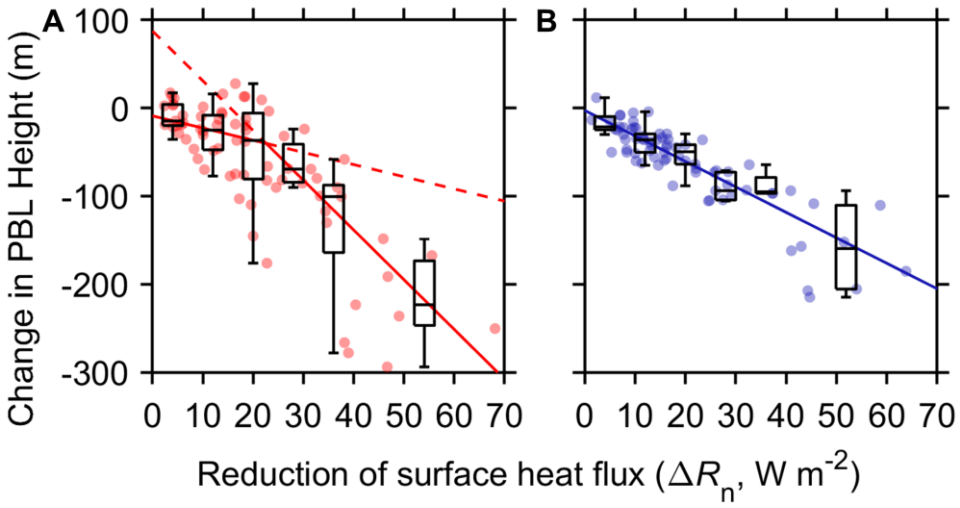

Figure S15: Aerosol induced PBL height change as a function of reduction in surface heat flux (the sum of sensible heat and latent heat) in the Beijing-Tianjin-Hebei, Henan-Shandong, and Yangtze River Delta regions

The data are adopted from a regional WRF-Chem simulations of Ding *et al.*[23]. A) The effect of reducing black carbon (BC) (SSA=0.85). In the presence of BC aerosols, the change of PBL height shows a much weaker dependence on ΔR_n at ΔR_n < ~ 20 W m^{-2} than that of pure scattering aerosols, but becomes much more sensitive at ΔR_n > ~ 20 W m^{-2}. Here, the abrupt change of PBL height is not as pronounced as in single column model simulations because it is a statistic of all domain grids and simulation time points from a regional WRF-Chem simulations of Ding *et al.* [23]. B) The effect of reducing pure scattering aerosols (SSA=1). With pure scattering aerosols, the change of PBL height shows a moderate nearly linear dependence on the reduction of surface heat flux (ΔR_n).

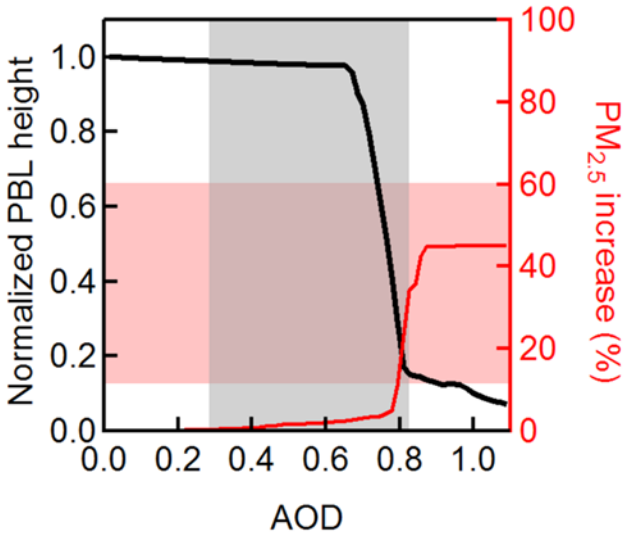

Figure S16: Impact of aerosol-induced prompt transition on surface $PM_{2.5}$ concentration

WRF-Chem simulated maximum PBL height and $PM_{2.5}$ increases. The black line represents the daily max PBL height and the red line represents the median value of normalized $PM_{2.5}$ concentration increase at 15:00 (local time) in WRF-Chem cases. The grey and red shadow show the uncertainty range (median value ± variance) of threshold initial $PM_{2.5}$ concentration and $PM_{2.5}$ increase with variations of initial meteorological conditions in Beijing, January 2013.

supplemental references

1. Sun, Y., Jiang, Q., Wang, Z., Fu, P., Li, J., Yang, T., and Yin, Y. (2014). Investigation of the sources and evolution processes of severe haze pollution in Beijing in January 2013. J. Geophys. Res-Atmos. *119*, 4380-4398. 10.1002/2014JD021641.
2. He, X., Li, C.C., Lau, A.K.H., Deng, Z.Z., Mao, J.T., Wang, M.H., and Liu, X.Y. (2009). An intensive study of aerosol optical properties in Beijing urban area. Atmos. Chem. Phys. *9*, 8903-8915. 10.5194/acp-9-8903-2009.
3. Garland, R.M., Schmid, O., Nowak, A., Achtert, P., Wiedensohler, A., Gunthe, S.S., Takegawa, N., Kita, K., Kondo, Y., Hu, M., et al. (2009). Aerosol optical properties observed during Campaign of Air Quality Research in Beijing 2006 (CAREBeijing-2006): Characteristic differences between the inflow and outflow of Beijing city air. J. Geophys. Res-Atmos. *114*. 10.1029/2008JD010780.
4. Lee, K.H., Li, Z., Wong, M.S., Xin, J., Wang, Y., Hao, W.-M., and Zhao, F. (2007). Aerosol single scattering albedo estimated across China from a combination of ground and satellite measurements. J. Geophys. Res-Atmos. *112*. 10.1029/2007JD009077.
5. Müller, D., Tesche, M., Eichler, H., Engelmann, R., Althausen, D., Ansmann, A., Cheng, Y.F., Zhang, Y.H., and Hu, M. (2006). Strong particle light absorption over the Pearl River Delta (south China) and Beijing (north China) determined from combined Raman lidar and Sun photometer observations. Geophys. Res. Lett. *33*, 10.1029/2006GL027196.
6. Cheng, T., Xu, C., Duan, J., Wang, Y., Leng, C., Tao, J., Che, H., He, Q., Wu, Y., Zhang, R., et al. (2015). Seasonal variation and difference of aerosol optical properties in columnar and surface atmospheres over Shanghai. Atmos. Environ. *123*, 315-326. 10.1016/j.atmosenv.2015.05.029.
7. Xu, J., Bergin, M.H., Yu, X., Liu, G., Zhao, J., Carrico, C.M., and Baumann, K. (2002). Measurement of aerosol chemical, physical and radiative properties in the Yangtze delta region of China. Atmos. Environ. *36*, 161-173. 10.1016/S1352-2310(01)00455-1.
8. Garland, R.M., Yang, H., Schmid, O., Rose, D., Nowak, A., Achtert, P., Wiedensohler, A., Takegawa, N., Kita, K., Miyazaki, Y., et al. (2008). Aerosol optical properties in a rural environment near the mega-city Guangzhou, China: implications for regional air pollution, radiative forcing and remote sensing. Atmos. Chem. Phys. *8*, 5161-5186. 10.5194/acp-8-5161-2008.
9. Wu, D., Mao, J., Deng, X., Tie, X., Zhang, Y., Zeng, L., Li, F., Tan, H., Bi, X., Huang, X., et al. (2009). Black carbon aerosols and their radiative properties in the Pearl River Delta region. Sci. China Ser. D. *52*, 1152-1163. 10.1007/s11430-009-0115-y.
10. Cui, F., Chen, M., Ma, Y., Zheng, J., Yao, L., and Zhou, Y. (2016). Optical properties and chemical apportionment of summertime PM2.5 in the suburb of Nanjing. J. Atmos. Chem. *73*, 119-135. 10.1007/s10874-015-9313-5.
11. Zhuang, B., Wang, T., Liu, J., Li, S., Xie, M., Han, Y., Chen, P., Hu, Q., Yang, X.-Q., Fu, C., et al. (2017). The surface aerosol optical properties in the urban area of Nanjing, west Yangtze River Delta, China. Atmos. Chem. Phys. *17*, 1143-1160. 10.5194/acp-17-1143-2017.

12. Yu, X., Ma, J., Kumar, K.R., Zhu, B., An, J., He, J., and Li, M. (2016). Measurement and analysis of surface aerosol optical properties over urban Nanjing in the Chinese Yangtze River Delta. Sci. Total Environ. *542*, 277-291. 10.1016/j.scitotenv.2015.10.079.

13. Shen, Y., Virkkula, A., Ding, A., Wang, J., Chi, X., Nie, W., Qi, X., Huang, X., Liu, Q., Zheng, L., et al. (2018). Aerosol optical properties at SORPES in Nanjing, east China. Atmos. Chem. Phys. *18*, 5265-5292. 10.5194/acp-18-5265-2018.

14. Wang, J., Virkkula, A., Gao, Y., Lee, S., Shen, Y., Chi, X., Nie, W., Liu, Q., Xu, Z., Huang, X., et al. (2017). Observations of aerosol optical properties at a coastal site in Hong Kong, South China. Atmos. Chem. Phys. *17*, 2653-2671.10.5194/acp-17-2653-2017.

15. Wu, Y., Zhang, R., Pu, Y., Zhang, L., Ho, K.F., and Fu, C. (2012). Aerosol optical properties observed at a semi-arid rural site in Northeastern China. Aerosol Air Qual. Res. *12*, 503-514. 10.4209/aaqr.2011.11.0202.

16. Virkkula, A., Backman, J., Aalto, P.P., Hulkkonen, M., Riuttanen, L., Nieminen, T., dal Maso, M., Sogacheva, L., de Leeuw, G., and Kulmala, M. (2011). Seasonal cycle, size dependencies, and source analyses of aerosol optical properties at the SMEAR II measurement station in Hyytiälä, Finland. Atmos. Chem. Phys. *11*, 4445-4468. 10.5194/acp-11-4445-2011.

17. Sherman, J.P., Sheridan, P.J., Ogren, J.A., Andrews, E., Hageman, D., Schmeisser, L., Jefferson, A., and Sharma, S. (2015). A multi-year study of lower tropospheric aerosol variability and systematic relationships from four North American regions. Atmos. Chem. Phys. *15*, 12487-12517. 10.5194/acp-15-12487-2015.

18. Delene, D.J. and Ogren, J.A. (2002). Variability of aerosol optical properties at four north American surface monitoring sites. J. Atmos. Sci. *59*, 1135-1150. 10.1175/1520-0469.

19. Ma, N., Birmili, W., Müller, T., Tuch, T., Cheng, Y.F., Xu, W.Y., Zhao, C.S., and Wiedensohler, A. (2014). Tropospheric aerosol scattering and absorption over central Europe: a closure study for the dry particle state. Atmos. Chem. Phys. *14*, 6241-6259. 10.5194/acp-14-6241-2014.

20. Kaminski, U. (2006). Aktuelle aerosoltrends an der GAW globalstation hohenpeißenberg und ihre relevanz für luftreinhaltung und klima. Uwsf. *18*, 88-94. 10.1007/bf03177639

21. Wang, Z., Huang, X., and Ding, A. (2018). Dome effect of black carbon and its key influencing factors: a one-dimensional modelling study. Atmos. Chem. Phys. *18*, 2821-2834. 10.5194/acp-18-2821-2018.

22. Su, T., Li, Z., Li, C., Li, J., Han, W., Shen, C., Tan, W., Wei, J., and Guo, J. (2020). The significant impact of aerosol vertical structure on lower atmosphere stability and its critical role in aerosol–planetary boundary layer (PBL) interactions, Atmos. Chem. Phys., *20*, 3713-3724. 10.5194/acp-20-3713-2020.

23. Ding, A., Huang, X., Nie W., Sun, J., Kerminen, V.-M., Petäjä, T., Su, H., Cheng, Y., Yang, X.-Q., Wang, M., et al. (2016). Enhanced haze pollution by black carbon in megacities in China. Geophys. Res. Lett. *43*, 2873-2879. 10.1002/2016GL067745.